

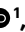








# p38 $\gamma$ / $\delta$ activation alters cardiac electrical activity and predisposes to ventricular arrhythmia

Received: 11 January 2023

Accepted: 19 October 2023

Published online: 27 November 2023

 Check for updates


Rafael Romero-Becerra <sup>1</sup>, Francisco M. Cruz<sup>1</sup>, Alfonso Mora <sup>1</sup>, Juan Antonio Lopez<sup>1,2</sup>, Daniela Ponce-Balbuena<sup>3</sup>, Andrew Allan<sup>3</sup>, Roberto Ramos-Mondragón<sup>3</sup>, Bárbara González-Terán <sup>1,4</sup>, Marta León<sup>1</sup>, Maria Elena Rodríguez<sup>1</sup>, Luis Leiva-Vega<sup>1</sup>, Guadalupe Guerrero-Serna<sup>3</sup>, Eric N. Jimenez-Vazquez<sup>3</sup>, David Filgueiras-Rama <sup>1,2,5</sup>, Jesús Vázquez <sup>1,2</sup>, José Jalife <sup>1,2,3</sup>  & Guadalupe Sabio <sup>1</sup> 

Ventricular fibrillation (VF) is a leading immediate cause of sudden cardiac death. There is a strong association between aging and VF, although the mechanisms are unclear, limiting the availability of targeted therapeutic interventions. Here we found that the stress kinases p38 $\gamma$  and p38 $\delta$  are activated in the ventricles of old mice and mice with genetic or drug-induced arrhythmogenic conditions. We discovered that, upon activation, p38 $\gamma$  and p38 $\delta$  cooperatively increase the susceptibility to stress-induced VF. Mechanistically, our data indicate that activated p38 $\gamma$  and p38 $\delta$  phosphorylate ryanodine receptor 2 (RyR2) disrupt Kv4.3 channel localization, promoting sarcoplasmic reticulum calcium leak,  $I_{to}$  current reduction and action potential duration prolongation. In turn, this led to aberrant intracellular calcium handling, premature ventricular complexes and enhanced susceptibility to VF. Blocking this pathway protected genetically modified animals from VF development and reduced the VF duration in aged animals. These results indicate that p38 $\gamma$  and p38 $\delta$  are a potential therapeutic target for sustained VF prevention.

Cardiovascular diseases (CVDs) remain the leading cause of death globally. Sudden cardiac death accounts for more than 60% of all deaths from CVD, being the most common cause of death worldwide<sup>1,2</sup>. Most deaths that meet the definition of sudden cardiac death are caused by cardiac arrhythmias<sup>2,3</sup>. Although atrial fibrillation (AF) is the most common type of sustained cardiac arrhythmia, ventricular fibrillation (VF) is one of the leading rhythm alterations documented at the time of medical assistance in patients with cardiac arrest<sup>4</sup>. Aging is a well-known risk factor for arrhythmia development, including AF and VF<sup>3,5,6</sup>. Despite ongoing efforts in treatment and prevention, the continuous

growth of the elderly population and the increasing prevalence of cardiac arrhythmia, also in younger adults<sup>7</sup>, is turning the management of severe ventricular arrhythmias into a serious public health problem. There are limited pharmacological and invasive therapeutic strategies to effectively prevent or treat the most lethal ventricular arrhythmia. Moreover, patients with implantable defibrillators (which may terminate a lethal arrhythmic event) are not exempt from important comorbidities, including important psychological effects<sup>8</sup>. Consequently, there is an urgent need to investigate the underlying molecular mechanisms toward developing more effective strategies to treat and

<sup>1</sup>Centro Nacional de Investigaciones Cardiovasculares (CNIC), Madrid, Spain. <sup>2</sup>CIBER de Enfermedades Cardiovasculares (CIBERCIV), Madrid, Spain.

<sup>3</sup>Center for Arrhythmia Research, Department of Internal Medicine, University of Michigan, Ann Arbor, MI, USA. <sup>4</sup>Gladstone Institutes, San Francisco, CA, USA. <sup>5</sup>Hospital Clínico Universitario San Carlos, Madrid, Spain.  e-mail: [jose.jalife@cnic.es](mailto:jose.jalife@cnic.es); [gsabio@cnic.es](mailto:gsabio@cnic.es)

prevent potentially lethal ventricular arrhythmias in specific population subsets.

p38 MAPKs are stress-activated protein kinases that respond to various cellular stress stimuli, including hypoxia, oxidative stress, inflammatory cytokines and muscle contraction<sup>9</sup>. This family consists of four family members—p38 $\alpha$ ,  $\beta$ ,  $\gamma$  and  $\delta$ —with p38 $\alpha$  being the most broadly studied, whereas knowledge about the other members is limited. Despite sharing structural similarities and signaling activation, as well as having similar target consensus sequences, each family member can exhibit distinct functions and regulatory mechanisms. Notably, p38 $\alpha$  and p38 $\beta$  share common substrates, and p38 $\gamma$  and p38 $\delta$  also share substrates between themselves. However, the number of substrates specific to all four family members is limited, indicating a potential segregation of the p38 signaling pathway into two distinct branches. One branch includes p38 $\alpha$  and p38 $\beta$ , each with its own set of substrates and functions, whereas the other branch consists of p38 $\gamma$  and p38 $\delta$ , featuring unique substrates and functions<sup>9,10</sup>. In cardiomyocytes, these two branches also exhibit distinctive activation mechanisms. The phosphorylation of p38 $\alpha$  and p38 $\beta$  is mainly mediated by MKK6 activation, whereas the activation of p38 $\gamma$  and p38 $\delta$  involves MKK3 phosphorylation<sup>11</sup>. Interestingly, when MKK6 is absent, there is a compensatory mechanism at play. This involves the upregulation and activation of MKK3, leading to the activation of p38 $\gamma$  and p38 $\delta$  family members. These findings highlight the intricate and dynamic regulatory network of the p38 signaling pathway in cardiomyocytes, with distinct branches being activated under different conditions or in response to specific stimuli.

In light of the evidence linking the activation of stress kinases, such as p38 and JNK2, with heart failure<sup>12</sup>, the cardiac response to angiotensin II (ref. 13) and age-related enhanced atrial arrhythmia susceptibility<sup>14</sup>, we sought to investigate whether the p38 branch of stress-activated kinases could also be involved in ventricular arrhythmia susceptibility under various disease conditions.

Here we demonstrate that p38 $\gamma/\delta$  are central regulators of cardiac electrical activity. Our results show that p38 $\gamma/\delta$  phosphorylation is increased in aged mouse hearts as well as in other mouse models associated with cardiac arrhythmia. Activation of p38 $\gamma/\delta$  in the heart increases susceptibility to stress-induced ventricular tachycardia (VT) and VF. We identified ryanodine receptor 2 (RyR2), a key channel for the release of Ca<sup>2+</sup> from the sarcoplasmic reticulum (SR) during cardiac contraction<sup>15</sup>, as a direct target of p38 $\gamma/\delta$  phosphorylation. Activated p38 $\gamma/\delta$  directly phosphorylate RyR2, and disrupt Kv4.3 channel localization, promoting SR Ca<sup>2+</sup> leak and action potential duration (APD) prolongation. The latter promoted ectopic activity and stress-induced ventricular arrhythmias in live mice. p38 $\gamma$  removal normalized RyR2 phosphorylation and reduced susceptibility to VT/VF. These data establish p38 $\gamma/\delta$  as central mediators of stress-induced cardiac electrical adaptation, suggesting their inhibition as a potential target for new therapeutic approaches in the management of ventricular arrhythmias.

## Results

### p38 $\gamma/\delta$ is hyperactivated in the aging heart and in arrhythmogenic animal models

Aging is associated with an increased prevalence of cardiac arrhythmias, which contribute to higher morbidity and mortality in the elderly<sup>5</sup>. Interestingly, immunoblot analysis of p38 expression and activation in cardiac tissue showed that p38 $\gamma/\delta$  phosphorylation was increased in old wild-type (WT) mice compared with young animals, whereas no changes in p38 $\alpha/\beta$  phosphorylation were observed (Fig. 1a and Extended Data Fig. 1). Then, we further explored if p38 $\gamma/\delta$  were also phosphorylated in other mouse models of acquired or inherited cardiac arrhythmia. Isoproterenol (ISO) is a  $\beta$ -adrenoceptor agonist that has been widely used to induce arrhythmias in both humans and animals<sup>16</sup>. We observed increased phosphorylation levels of p38 $\gamma/\delta$  in hearts from WT mice 15 min after ISO administration (Fig. 1b). Similarly, after 30 min of ISO

treatment, human induced pluripotent stem cell (hiPSC)-differentiated cardiomyocytes showed increased phosphorylation of p38 $\gamma/\delta$  (Fig. 1c). We also checked if p38 $\gamma/\delta$  activation was also present in genetic mouse models of human cardiac disease. Mutations in the myosin-binding protein C (cMyBP-C) gene are involved in the development of familial hypertrophic cardiomyopathy<sup>17</sup>, and cMyBP-C-deficient mice develop dilated cardiomyopathy<sup>18</sup> and are susceptible to ventricular arrhythmia<sup>19</sup>. Immunoblot analysis of heart lysates from cMyBP-C null mice showed that p38 $\gamma$  expression was increased in the heart of these animals compared with control hearts (Fig. 1d). Similarly, the lamin A mutant mice *Lmna*<sup>G609G/G609G</sup>, which develop progeria, repolarization alterations and a higher ventricular arrhythmia burden compared with controls<sup>20</sup>, also showed increased levels of p38 $\gamma$  in the heart (Fig. 1e). Taken together, these results suggest that p38 $\gamma/\delta$  activation is a common feature in different disease conditions and may contribute to an increased risk of ventricular arrhythmia.

### Cardiac p38 $\gamma/\delta$ activation promotes a pro-arrhythmic phosphoproteome profile and RyR2 phosphorylation

To explore the signaling network triggered by the activation of p38 $\gamma/\delta$  in the heart, we infected 2-month-old WT mice with adeno-associated viruses with cardiac troponin T promoter (AAV-cTnT) driving expression of either constitutively active p38 $\gamma$  and p38 $\delta$  kinases (cTnT-p38 $\gamma^*/\delta^*$ ) or GFP as a control (cTnT-GFP) (Fig. 2a). The level of phosphorylation observed in cTnT-p38 $\gamma^*/\delta^*$  hearts was similar to the physiological levels found in the hearts of old WT mice (Extended Data Fig. 2a). We first explored whether cardiac p38 $\gamma^*/\delta^*$  expression increased susceptibility to stress-induced AF and VF by adrenergic stimulation and invasive electrophysiological testing using an intracardiac catheter burst pacing. We found that programmed stimulation induced a significantly higher incidence of AF in cTnT p38 $\gamma^*/\delta^*$ -infected mice compared with cTnT-GFP-infected mice, with a significantly increased sensitivity to  $\beta$ -adrenergic stimulation (ISO) (Extended Data Fig. 2b). Notably, we also found a significantly higher incidence of VT/VF, one of the most life-threatening arrhythmias<sup>4</sup>, in cTnT p38 $\gamma^*/\delta^*$ -infected mice (Fig. 2b,c). To further investigate the individual contributions of p38 $\gamma$  and p38 $\delta$  isoforms, we evaluated the susceptibility to stress-induced VT/VF in WT mice injected with AAV-TnT viruses expressing the single kinases separately. Consistent with our previous findings, which indicate cooperation of both kinases in the signaling pathway<sup>13,21</sup>, mice infected with viruses expressing either p38 $\gamma$  or p38 $\delta$  alone exhibited a lower burden of VT/VF compared with mice simultaneously infected with viruses expressing both p38 $\gamma$  and p38 $\delta$  (Extended Data Fig. 2c). These results suggest that the combined activity of p38 $\gamma$  and p38 $\delta$  isoforms may contribute to a higher susceptibility to ventricular arrhythmias.

To decipher how the activation of these kinases contributes to the increased susceptibility to stress-induced VT/VF, we performed quantitative phosphoproteomics comparing cTnT-GFP and cTnT-p38 $\gamma^*/\delta^*$  hearts (Fig. 2a). Ingenuity Pathway Analysis (IPA)<sup>22</sup> of the differentially hyperphosphorylated proteins (DPhos) in cTnT-p38 $\gamma^*/\delta^*$ -infected hearts compared with control hearts showed that the top clinical pathologies identified were related to cardiac arrhythmia (Extended Data Fig. 2d and Supplementary Table 1). We found 86 differentially regulated phosphopeptides that mapped to a total of 28 proteins in the cardiac arrhythmia category (Extended Data Fig. 2e and Supplementary Table 2). These proteins were related to several arrhythmogenic diseases, including long-QT syndrome, familial arrhythmia and Wolff–Parkinson–White (WPW) syndrome (Extended Data Fig. 2f and Supplementary Table 3). We also noted that a large proportion of the measured proteome was also differentially regulated, and numerous hyperphosphorylated proteins also showed a higher expression in the cTnT-p38 $\gamma^*/\delta^*$  proteome (Extended Data Fig. 2e and Supplementary Table 4). To compensate for the contribution of protein expression changes, we expressed the changes in phosphopeptide abundance

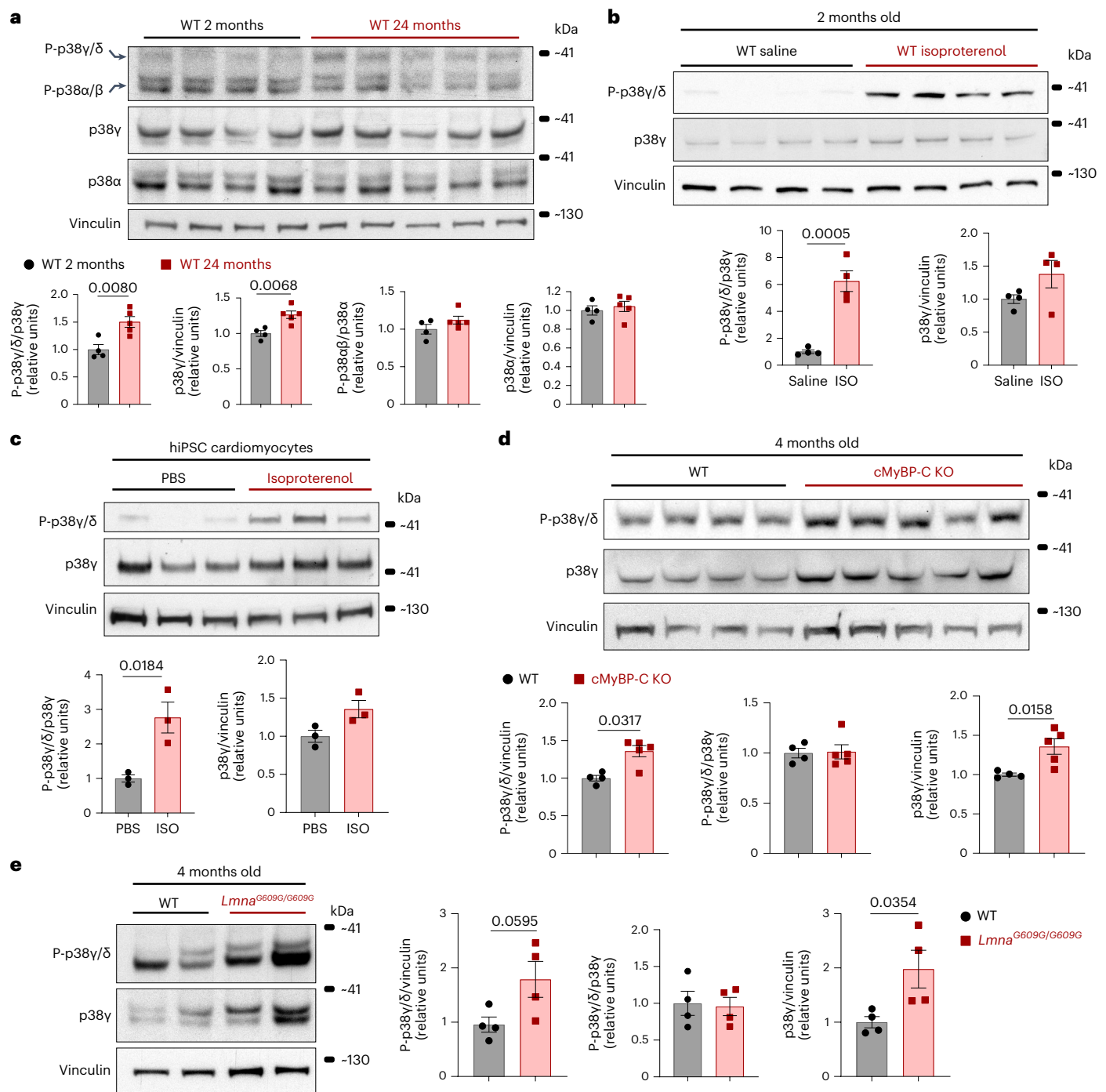


**Fig. 1 | Immunoblot evaluation of p38γ/δ expression and phosphorylation with aging and in pro-arrhythmogenic models. a**, Immunoblot analysis of the phosphorylation and protein levels of the different p38 family members in ventricles from 2-month-old ( $n = 4$ ) and 24-month-old ( $n = 4$ ) WT male mice. Two-sided unpaired Student's *t*-test or Mann–Whitney *U*-test. **b**, Phosphorylation and protein levels of p38γ/δ evaluated by immunoblot in ventricles from 2-month-old WT mice treated with saline ( $n = 4$ ) or isoproterenol ( $n = 4$ ). Mice were injected i.p. with 20 mg kg<sup>-1</sup> ISO dissolved in saline. Exactly 15 min after injection, tissues were extracted and frozen in liquid N<sub>2</sub>. Two-sided unpaired Student's *t*-test.

**c**, Immunoblot analysis of the phosphorylation and protein levels of p38γ/δ in hiPSC-differentiated cardiomyocytes treated with PBS ( $n = 3$ ) or ISO ( $n = 3$ ) 1 μM for 30 min. Two-sided unpaired Student's *t*-test. **d**, Immunoblot analysis of the phosphorylation and protein levels of p38γ/δ in the ventricles from 4-month-old WT ( $n = 4$ ) and cMyBP-C KO ( $n = 5$ ) mice. Two-sided unpaired Student's *t*-test or Mann–Whitney *U*-test. **e**, Immunoblot analysis of the phosphorylation and protein levels of p38γ/δ in the ventricles from 4-month-old WT ( $n = 4$ ) and *Lmna*<sup>G609G/G609G</sup> ( $n = 4$ ) mice. Two-sided unpaired Student's *t*-test. Data are expressed as mean ± s.e.m.

in relation to the proteins they came from using an advanced statistical model specifically developed to study post-translational modifications<sup>23</sup> before performing the significance analysis. IPA using the corrected phosphoproteome data highlighted cardiac dysfunction and cardiac arrhythmia as the top clinical pathologies identified

(Fig. 2d and Supplementary Table 5). We identified 15 corrected phosphopeptides that mapped to seven proteins in the cardiac arrhythmia category, which were related to arrhythmogenic diseases such as long-QT syndrome, familial arrhythmia, VF and WPW syndrome (Fig. 2e and Supplementary Tables 6 and 7). Notably, the top

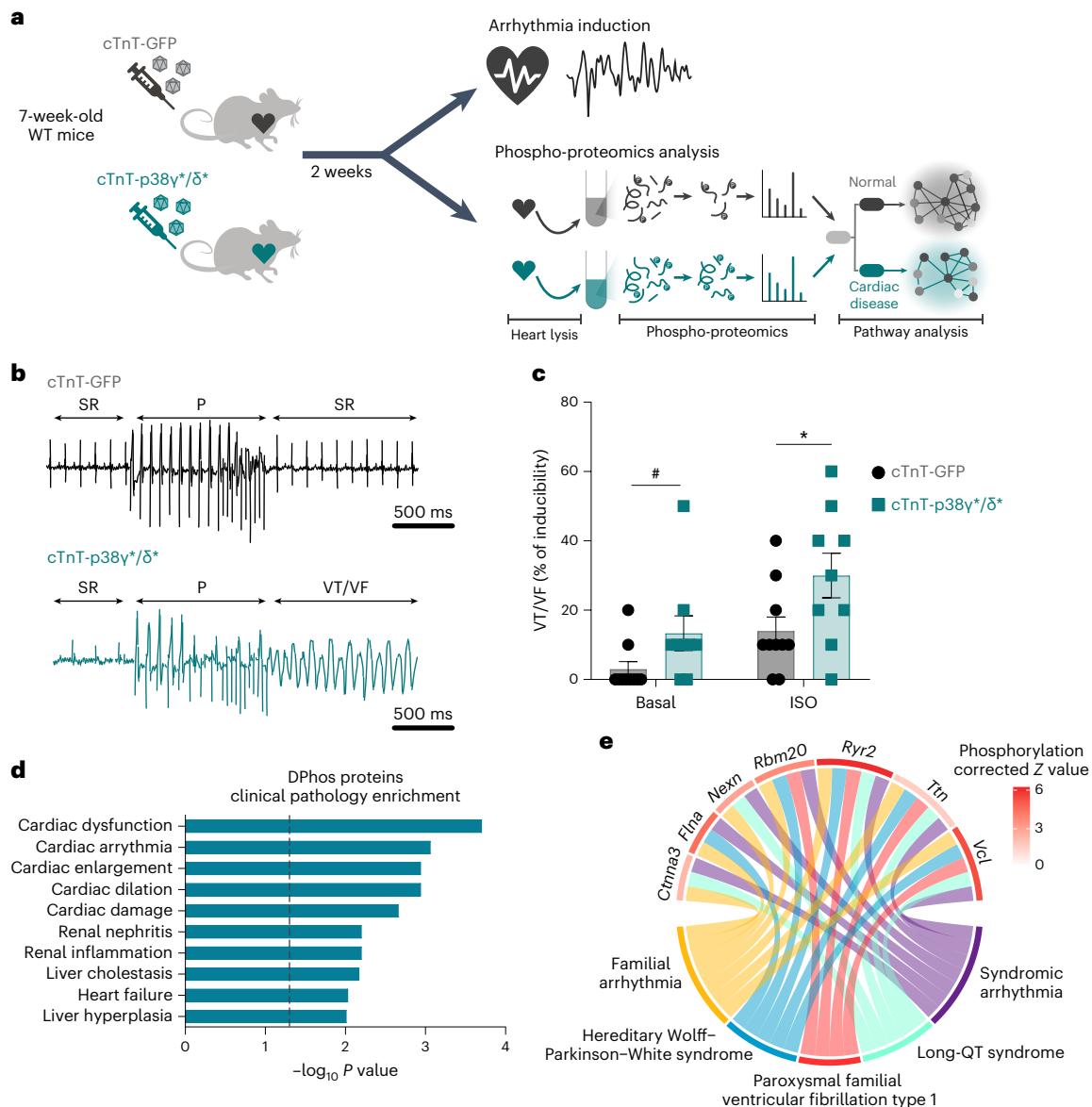


**Fig. 2 | p38 $\gamma/\delta$  activation increases the susceptibility to stress-induced VF and a pro-arrhythmic cardiac phosphoproteome profile. a**, Strategy for arrhythmia induction and unbiased mass spectrometry phosphoproteomics analysis of hearts lysates. At 7 weeks of age, WT mice received intravenously systemic administration of AAV encoding constitutively active p38 $\gamma/\delta$  kinases (cTnT-p38 $\gamma^*/\delta^*$ ,  $n = 3$ ) or a GFP protein as a control (cTnT-GFP,  $n = 4$ ) under the chicken cardiac troponin T (*TNN2*) promoter. Two weeks after AAV administration, a set of mice was used for arrhythmia induction by intracardiac stimulation, and the hearts from another set of mice were extracted for phosphoproteomics analysis. Frozen hearts were homogenized in lysis buffer and then subjected to trypsin digestion and prepared for isobaric labeling and phosphopeptide enrichment. Labeled peptides were then analyzed by LC-MS/MS. Differentially hyperphosphorylated peptides ( $Z$  value difference  $> 0$ , two-sided limma  $t$ -test  $P < 0.05$ ) were then used for pathway analysis. **b**, Surface lead-II ECGs during sinus rhythm (SR) and intracardiac rapid pacing (P) in anesthetized

cTnT-GFP and cTnT-p38 $\gamma^*/\delta^*$  mice. In basal and after ISO administration (i.p. 5 mg kg $^{-1}$ ), a brief train of intracardiac ventricular pacing stimuli triggered an episode of VT/VF. **c**, Percentage of VT/VF inducibility by S1-S2 protocol 1 (Methods) in cTnT-GFP ( $n = 10$ ) and cTnT-p38 $\gamma^*/\delta^*$  ( $n = 9$ ) mice in the absence (basal) and presence (ISO) of isoproterenol. Each dot shows the percentage of VT/VF induced in each mouse by the S1-S2 protocol. \* $P = 0.0353$ , two-way ANOVA followed by Sidak's post test; # $P = 0.0186$ , two-sided Mann-Whitney  $U$ -test. Data are expressed as mean  $\pm$  s.e.m. **d**, Clinical pathology enrichment (Tox Functions) of the differentially hyperphosphorylated proteins ( $Z$  value difference  $> 0$ ; limma two-sided  $t$ -test  $P < 0.05$ ) from cTnT-p38 $\gamma^*/\delta^*$  hearts compared with controls, as determined by IPA. The vertical dashed line indicates the threshold of  $-\log_{10}$  (two-sided Fisher's exact test  $P$  value) = 1.3. **e**, Chord diagram of the phosphoproteins found in the category 'Cardiac Arrhythmia' shown in **d**, and the five most significant pathologies in this category to which the phosphoproteins are assigned. Proteins are identified by their gene name for simplicity.

differentially hyperphosphorylated site in cTnT-p38 $\gamma^*/\delta^*$ -infected hearts compared with controls was S2367 of RyR2 (Fig. 3a,b and Supplementary Table 6). RyR2 is a key protein for the control of cardiac calcium handling and cardiac contraction. Mutations in this channel are associated with the development of ventricular arrhythmias<sup>15,24</sup>. Furthermore, RyR2 phosphorylation is a key mechanism to control channel activity, and alterations in RyR2 phosphorylation participate in several

cardiac diseases, including ventricular arrhythmia and sudden death<sup>25</sup>. Hence, we decided to explore RyR2 as an interesting p38 $\gamma/\delta$  potential target. We verified the direct phosphorylation of RyR2 by p38 $\gamma/\delta$  in an in vitro kinase assay with recombinant p38 $\gamma/\delta$  proteins but not by p38 $\alpha$  or p38 $\beta$  (Fig. 3c and Extended Data Fig. 3a). Immunoblot analysis confirmed that cardiomyocyte-specific expression of constitutively active p38 $\gamma/\delta$  also led to RyR2 phosphorylation at P-Ser p38 motif in



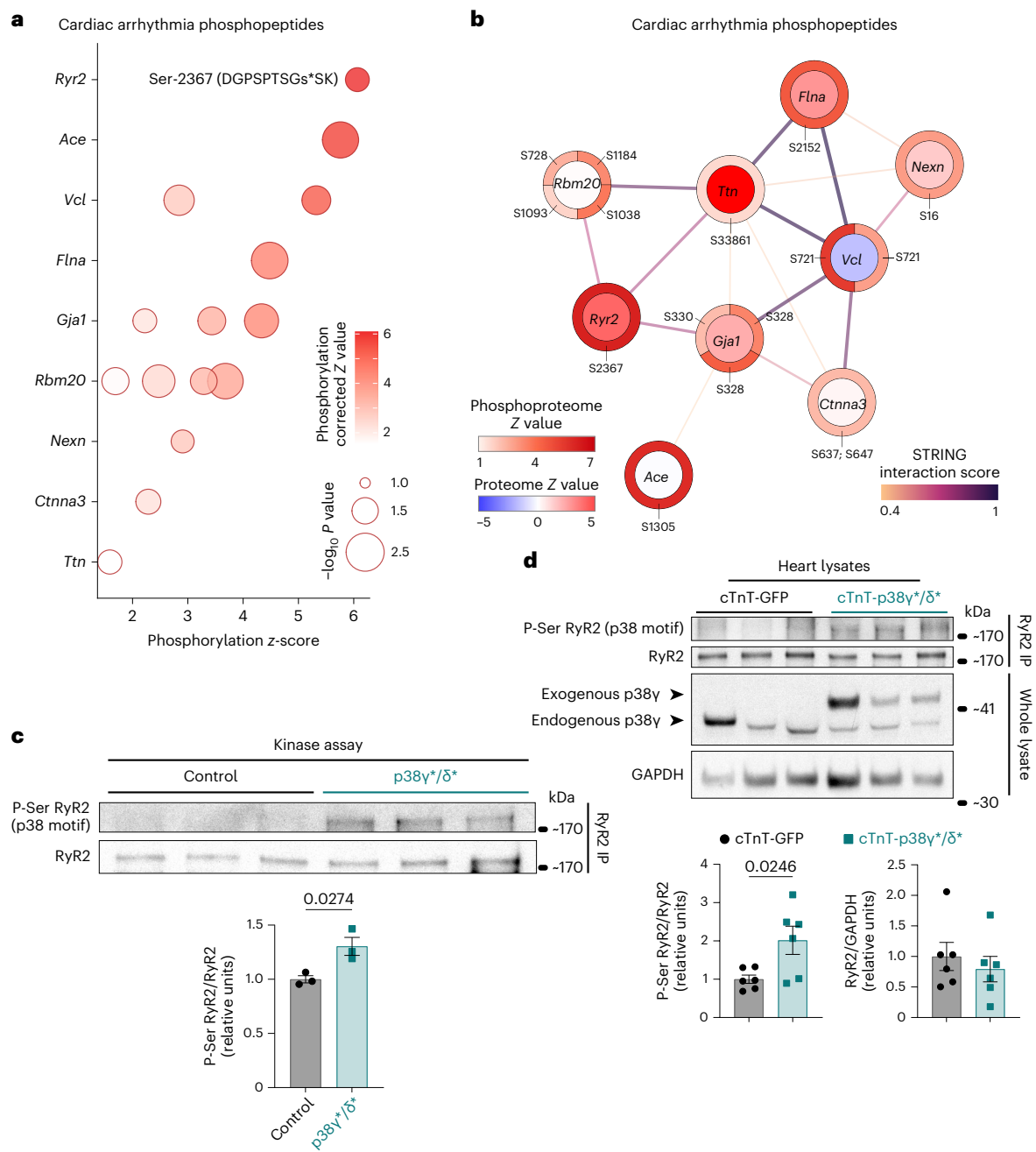


**Fig. 3 | Identification of RyR2 as a direct target of p38 $\gamma/\delta$ .** **a**, Bubble plot showing the phosphorylation Z value and P value of the phosphopeptides involved in the category ‘Cardiac Arrhythmia’ shown in Fig. 2d. Each dot corresponds to the different phosphopeptides in each protein. Only significant (Z value difference > 0; two-sided limma *t*-test  $P < 0.05$ ) phosphopeptides are presented. Proteins are defined by their gene name for simplicity. **b**, Interaction network of differentially phosphorylated proteins involved in the category ‘Cardiac Arrhythmia’ shown in **a**, based on STRING database and visualized in Cytoscape. The node colors indicate the differential abundance (inner circle) and corrected phosphorylation state (outer circle) of the proteins in cTnT-p38 $\gamma^*/\delta^*$  versus cTnT-GFP hearts. Small numbers pointing to segments of the

outer circles indicate the position of the phosphosite in the sequence of the protein. The color of the edges indicates the STRING interaction score between proteins. Only significant (Z value difference > 0; two-sided limma *t*-test  $P < 0.05$ ) phosphopeptides are indicated. Proteins are defined by their gene name for simplicity. **c**, In vitro phosphorylation kinase assay of RyR2 isolated from mice hearts on P-Ser p38 motif by active recombinant p38 $\gamma$  and p38 $\delta$  ( $n = 3$ ). Two-sided unpaired Student’s *t*-test. **d**, RyR2 phosphorylation at P-Ser p38 sites as assessed by immunoprecipitation of heart lysates from cTnT-GFP ( $n = 6$ ) and cTnT-p38 $\gamma^*/\delta^*$  ( $n = 6$ ) mice. Arrowheads indicate exogenous (top) and endogenous (bottom) p38 $\gamma$ . Two-sided unpaired Student’s *t*-test. Data are expressed as mean  $\pm$  s.e.m. IP, immunoprecipitation.

vivo (Fig. 3d). Remarkably, RyR2 also presented increased phosphorylation at P-Ser p38 motif in 24-month-old WT mice compared with young mice (Extended Data Fig. 3b). Altogether, these results indicate that p38 $\gamma/\delta$  activation increases the risk of potentially lethal ventricular arrhythmia and suggest that RyR2 hyperphosphorylation might be involved in the underlying mechanisms.

### p38 $\gamma/\delta$ hyperactivation promotes RyR2 phosphorylation and ventricular arrhythmia in MKK6 knockout mice

We recently demonstrated that the deletion of MKK6, an upstream p38 $\alpha$  activator, promotes the activation of p38 $\gamma/\delta$  in the heart<sup>11</sup>. Interestingly, MKK6 knockout (KO) (*Map2k6*<sup>-/-</sup>) mice show premature aging associated with phosphorylation of cardiac p38 $\gamma/\delta$ <sup>11</sup>. Because activation of

cardiac p38 $\gamma$ / $\delta$  induces ventricular arrhythmia and is also observed in aged mice (Fig. 1a and Extended Data Fig. 1), we decided to explore the contribution of p38 $\gamma$ / $\delta$  activation to ventricular arrhythmia in this mouse model.

First, we discarded fibrosis as a contributing substrate for arrhythmia susceptibility, as MKK6-deficient mice do not show cardiac fibrosis until very advanced age<sup>41</sup>.

As observed in cTnT-p38 $\gamma^*/\delta^*$  mice, activation of p38 $\gamma$ / $\delta$ <sup>11</sup> in 2-month-old MKK6 KO hearts correlates with increased phosphorylation of RyR2 at P-Ser p38 motif compared with WT hearts (Fig. 4a). This was accompanied by an increased susceptibility to stress-induced AF and VT/VF in MKK6 KO mice (Fig. 4b,c and Extended Data Fig. 4). All induced ventricular arrhythmias in MKK6 KO mice were polymorphic and lasted  $16 \pm 8$  s (range, 1–65 s). VT/VF terminated spontaneously in most MKK6 KO mice, although two cases led to death. The latter is remarkable in mice because long-lasting and lethal ventricular arrhythmia is rare in mouse models<sup>26,27</sup>.

To further explore the wave propagation alterations leading to arrhythmia initiation in MKK6 KO mice, we conducted optical mapping experiments in isolated Langendorff-perfused whole hearts. In the presence of ISO, three out of seven MKK6 KO hearts displayed frequent bursts of phase 2 and phase 3 early after-depolarizations (EADs; Fig. 4d,e) that deteriorated into VT/VF. Consistent with optical data from other animal models with VT/VF<sup>28</sup>, five out of seven MKK6 KO hearts sustained VT/VF by high-frequency rotational activity (Fig. 4f,g and Supplementary Video 1). Overall, the results indicate that, in MKK6-deficient hearts,  $\beta$ -adrenergic stimulation promotes EADs that, in some cases, are followed by sustained functional reentry in the form of electrical rotors generating spiral waves that maintain VT/VF.

RyR2 hyperphosphorylation has been associated with higher arrhythmogenic risk through increased Ca<sup>2+</sup> leak<sup>24,25,29</sup>. To evaluate whether this could be the mechanism triggering ventricular arrhythmia in MKK6 KO mice, we analyzed Ca<sup>2+</sup> handling in isolated cardiomyocytes from WT and MKK6 KO mice. Unlike WT cardiomyocytes, MKK6 KO myocytes subjected to  $\beta$ -adrenergic stimulation demonstrated impaired Ca<sup>2+</sup> transients with reduced amplitude increase in response to ISO. Under the same conditions, MKK6 KO myocytes also showed spontaneous Ca<sup>2+</sup> release events during the stimulus train and during the subsequent diastolic interval, consistent with EAD formation. Caffeine was then applied to measure basal SR Ca<sup>2+</sup> load (Fig. 5a,b). Decreased Ca<sup>2+</sup> transient amplitude in myocytes from MKK6 KO mice suggests depressed RyR2 function. This is in line with the results of our phosphoproteomics analysis indicating that the most significantly phosphorylated site in cTnT-p38 $\gamma^*/\delta^*$  hearts in RyR2 was Ser-2367 (Fig. 3a,b), which has been previously identified as an inhibitory phosphosite of RyR2 function<sup>30</sup>. This finding suggests that the p38 phosphorylation site on RyR2 functions as a negative regulator. Ca<sup>2+</sup> imaging experiments showed similar pacing-induced Ca<sup>2+</sup> transient and caffeine-induced Ca<sup>2+</sup> transient (SR Ca<sup>2+</sup> load) with no appearance of spontaneous Ca<sup>2+</sup> releases (SCRs) in the basal state. However, acute perfusion of ISO induced a significantly higher incidence of SCR events during and after pacing in MKK6 KO myocytes. ISO also induced higher diastolic Ca<sup>2+</sup> levels in MKK6 KO myocytes during the pacing, which reduced Ca<sup>2+</sup> transient amplitude. However, this was not translated into a reduced Ca<sup>2+</sup> fractional release in the pooled data (Fig. 5b). Our results indicate that p38 $\gamma$ / $\delta$  phosphorylation reduces RyR2 function, which, in the presence of stress (stimulation plus ISO), produces malignant arrhythmias, similarly to some RyR2 loss-of-function mutations that promote stress-induced VF due to spontaneous SR Ca<sup>2+</sup> release by a mechanism of store-overload-induced Ca<sup>2+</sup> release<sup>24,31–33</sup>.

Greater RyR2 leak with unchanged SR content could suggest a faster SR calcium reuptake by SERCA2. To evaluate this possibility, we examined SERCA2 activity indirectly by assessing protein levels and phosphorylation of phospholamban (PLN), a key regulator of

SERCA2 (ref. 34). Previous evidence implied p38 pathway in PLN phosphorylation at Thr-17 due to increased expression of CaMKII in cardiomyocytes<sup>35</sup>. Interestingly, we observed increased phosphorylation of PLN at Thr-17 and Ser-16, and decreased levels of PLN protein in MKK6 KO hearts, without changes in SERCA2 protein levels (Fig. 5c), suggesting reduced inhibition of SERCA2 activity.

Taken together, these results suggest that RyR2 phosphorylation due to p38 $\gamma$ / $\delta$  activation promotes abnormal spontaneous Ca<sup>2+</sup> transients, EADs and abnormal impulse propagation leading to reentry and fibrillation. Altogether, the data provide a robust mechanistic explanation for the increased susceptibility to stress-induced VT/VF observed in MKK6-deficient mice.

### MKK6 KO mice have reduced I<sub>to</sub> current, action potential prolongation and long QT

Ca<sup>2+</sup> leak from the SR due to RyR2 dysfunction is usually associated with delayed after-depolarizations<sup>15</sup>. However, SR Ca<sup>2+</sup> leak has also been shown to promote EADs and associated arrhythmias<sup>36–38</sup>. Because changes in other cardiac currents can contribute to EAD formation<sup>15</sup>, we performed voltage-clamp experiments in ventricular myocytes from WT and MKK6 KO mice to establish the underlying electrophysiologic mechanism of VT/VF initiation. Contrary to what we expected, I<sub>CaL</sub> calcium current was unchanged, or even reduced at –20 mV, in MKK6 KO cardiomyocytes compared with WT cardiomyocytes (Extended Data Fig. 5a). The results were similar for I<sub>Na</sub> sodium current (Extended Data Fig. 5b). Evaluation of total potassium current (I<sub>KT</sub>) showed that MKK6 KO cardiomyocytes showed a reduced potassium current only at the higher voltage values of the current–voltage relation (Fig. 6a). In agreement with this, I<sub>to</sub> (transient outward potassium current) was also reduced (Fig. 6b), but I<sub>K1</sub> (inward rectifier potassium current) was unchanged (Extended Data Fig. 5c), in MKK6 KO cardiomyocytes. We next examined how these changes in current density affected the action potential (AP) of the cardiomyocyte. Current-clamping of cardiomyocytes isolated from the left ventricular free wall revealed no significant differences in resting membrane potential, AP amplitude, overshoot or maximum rate of AP depolarization between WT and MKK6 KO cardiomyocytes (Extended Data Fig. 5d). However, the APD was prolonged in cardiomyocytes from MKK6 KO mice (Fig. 6c,d). This agrees with previous evidence showing that I<sub>to</sub> reduction in mice increases APD in isolated ventricular myocytes and prolongs the in vivo QT interval on the surface ECG<sup>39</sup>. Notably, the surface ECG of anesthetized animals also showed prolongation of the corrected QT interval and QRS interval in MKK6 KO mice (Fig. 6e,f). We then decided to investigate the molecular mechanism by which p38 $\gamma$ / $\delta$  activation could lead to I<sub>to</sub> reduction. The cardiac Kv4.2/3 channels responsible for I<sub>to</sub> current have been reported to interact with SAP97/Dlg1 (ref. 40), a scaffolding protein that is also a known phosphorylation target of p38 $\gamma$ <sup>41,42</sup>. In agreement with p38 $\gamma$  activation, the levels of phosphorylated SAP97 at the p38 T/P motif were increased in hearts lacking MKK6 (Fig. 6g). p38 $\gamma$ -dependent phosphorylation of SAP97 has been shown to modulate SAP97 cellular localization<sup>41,42</sup>. Additionally, SAP97 is a key partner for the surface expression of Kv4 channels<sup>40</sup>. Subcellular fractionation and immunoblot analysis showed that hearts from MKK6-deficient mice had a reduced localization of SAP97 and Kv4.3 in the plasma membrane fraction (Fig. 6h). Altogether, these results indicate that p38 $\gamma$  hyperactivation in MKK6 KO hearts promotes SAP97 hyperphosphorylation, reduction of SAP97 and Kv4.3 channel localization at the plasma membrane, consequently promoting I<sub>to</sub> reduction, with APD and QT prolongation.

### p38 $\gamma$ removal reduces susceptibility to arrhythmia in MKK6-deficient mice

Finally, to corroborate the key contribution of p38 $\gamma$  hyperphosphorylation to cardiac arrhythmia, we evaluated the vulnerability to stress-induced VT/VF in MKK6/p38 $\gamma$  DKO mice (*Map2k6*<sup>-/-</sup>; *Mapk12*<sup>-/-</sup>).

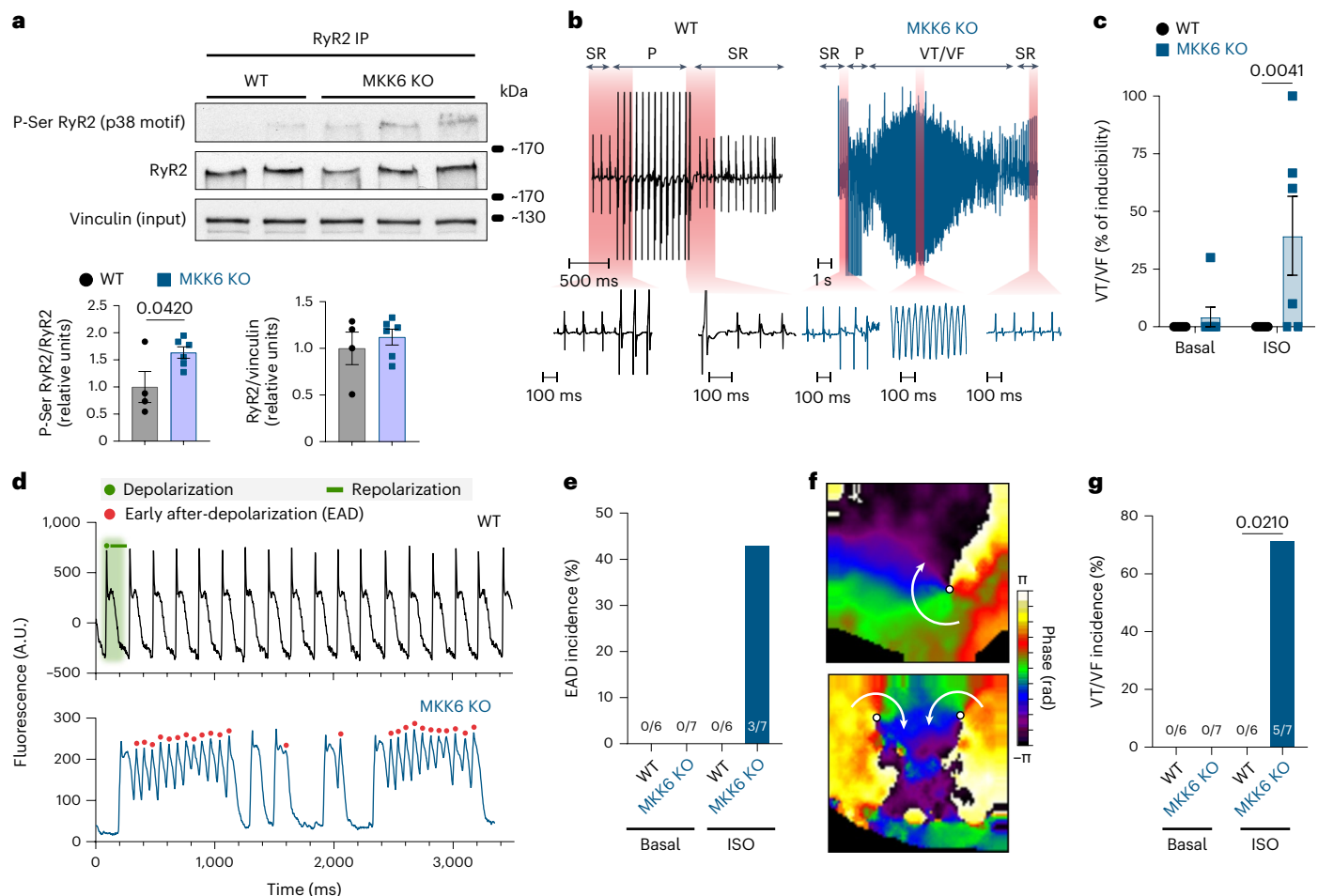


**Fig. 4 | p38 $\gamma$ / $\delta$  activation due to MKK6 deficiency promotes RyR2 hyperphosphorylation and ventricular arrhythmias. a**, Immunoblot evaluation of RyR2 phosphorylation at P-Ser p38 motif in heart lysates from 2-month-old MKK6 KO ( $n = 6$ ) and WT ( $n = 6$ ) mice (two-sided unpaired Student's *t*-test). **b**, Surface lead-II ECGs during sinus rhythm (SR) and intracardiac rapid pacing (P) in anesthetized WT and MKK6 KO mice. After ISO administration (i.p. 5 mg kg<sup>-1</sup>), a brief train of intracardiac ventricular pacing stimuli triggered a relatively long episode of VT/VF. Red shadows highlight regions for which expanded tracings are shown underneath. **c**, Percentage of VT/VF inducibility by S1-S2 protocol 2 (Methods) in WT ( $n = 7$  and  $7$ ) and MKK6 KO ( $n = 7$  and  $6$ ) mice in the absence (basal) and presence (ISO) of isoproterenol, respectively. Each dot shows the percentage of VT/VF induced in each mouse by the S1-S2 protocol 2. Two-way ANOVA followed by Sidak's post test. **d**, Representative optical membrane potential recordings (potentiometric dye Di-4-ANEPPS) from WT and MKK6 KO mouse hearts in the presence of ISO (300 nM) and high

$Ca^{2+}$  (2.5 mM). The WT heart responded 1:1 (stimulus:response) to electrical pacing at a cycle length of 300 ms via an octa-pole mouse catheter introduced through the right atria and making contact with the endocardial surface on the apex of the right ventricle. However, after the first stimulus, the MKK6 KO heart developed triggered activity with multiple episodes of EADs. **e**, Quantification of EAD incidence in MKK6 KO and WT mice in the presence (ISO) or absence (basal) of isoproterenol. **f**, Optical mapping phase maps of two different MKK6 KO hearts that developed VT/VF showing rotational activity in the form of a single and a pair of counter-rotating rotors (figure-eight reentry). To create the phase maps, each camera pixel was assigned to an instantaneous phase of the AP cycle (phase value between  $-\pi$  and  $+\pi$ ) for that given timepoint. **g**, Quantification of VT/VF incidence in optical mapping recordings of isolated WT and MKK6 KO hearts. The percentage of mice that developed VT/VF out of the total number of animals in each group is represented. Two-sided Fisher's exact test. Data in **a** and **c** are expressed as mean  $\pm$  s.e.m.

Although MKK6 KO mice were more susceptible than WT to VT/VF under basal conditions and with adrenergic stimulation, this susceptibility was significantly reduced when we evaluated the double mutant combination (Fig. 7a,b). Furthermore, this was accompanied by a reduction of RyR2 phosphorylation at P-Ser p38 motif in MKK6/p38 $\gamma$  DKO (Fig. 7c). We also evaluated if p38 $\gamma$  removal could protect aged animals from arrhythmia susceptibility in aged mice. Interestingly, we did not observe significant differences in arrhythmia susceptibility between WT and p38 $\gamma$  KO aged mice (Extended Data Fig. 6a). However, we did observe a shorter duration of arrhythmias in p38 $\gamma$  KO animals compared with WT mice (Extended Data Fig. 6b).

Altogether, our results identify p38 $\gamma$ / $\delta$  as important players in cardiac pathophysiology regulating the electrical function of the mouse cardiomyocyte. p38 $\gamma$ / $\delta$  phosphorylation results in the

phosphorylation of RyR2 and SAP97, promoting spontaneous calcium transients and reduced  $I_{to}$ . This results in APD prolongation, EADs and high-frequency rotational activity sustaining VF.

## Discussion

This study provides several independent lines of evidence collectively supporting a previously unrecognized role for the p38 $\gamma$ / $\delta$  signaling pathway in the control of electrical activity in the adult heart. We showed that these kinases become upregulated with age in the mouse heart and in other mouse models associated with cardiac arrhythmia. Activation of p38 $\gamma$ / $\delta$ , either through viral-mediated expression or MKK6 deficiency, promoted susceptibility to stress-induced malignant ventricular arrhythmias. Further molecular characterization linked p38 $\gamma$ / $\delta$  increased activation with RyR2 phosphorylation at Ser-2367

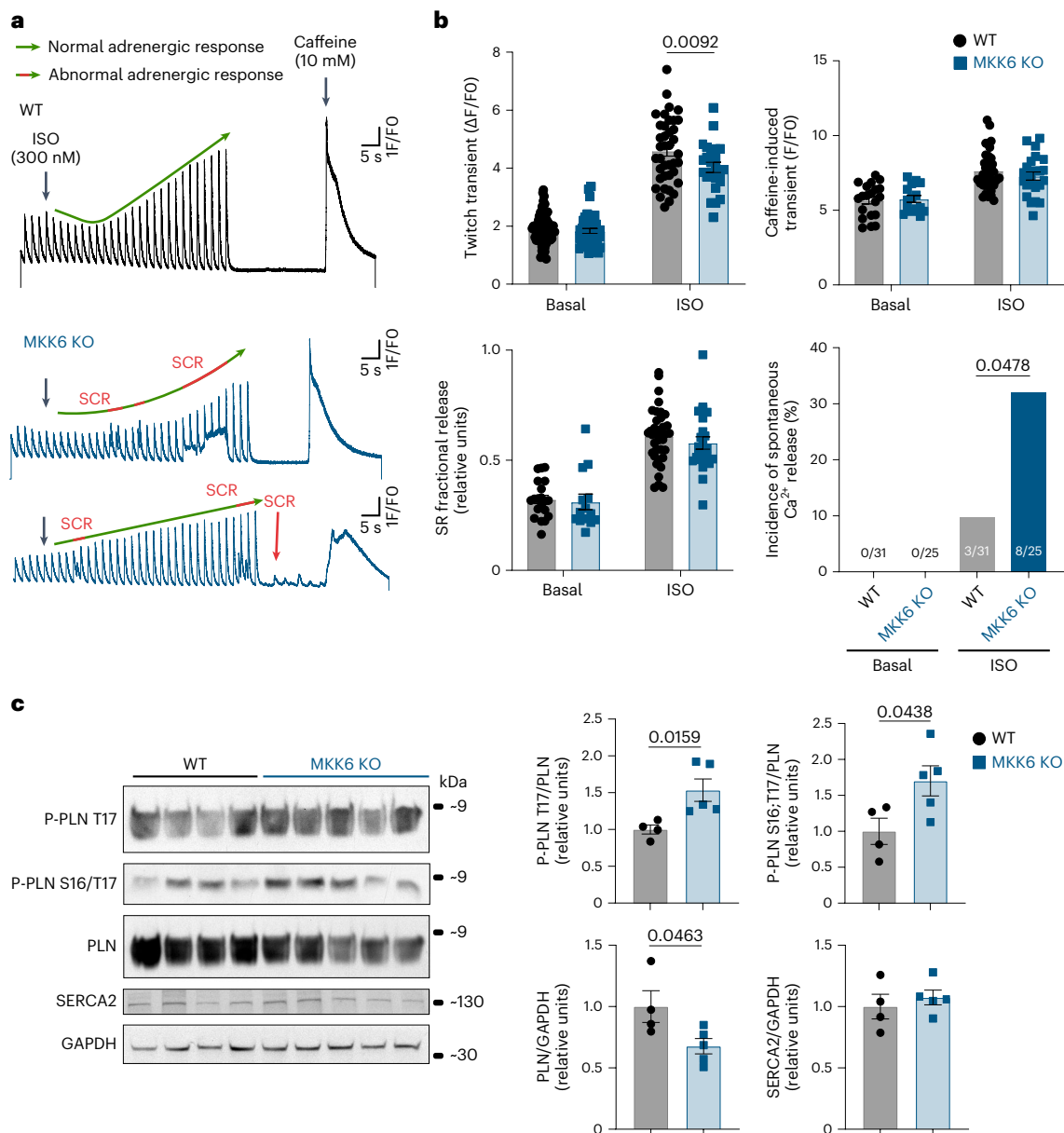


**Fig. 5 | MKK6-deficient cardiomyocytes are predisposed to ISO-induced abnormal SCR events.** **a**, Representative recordings of sarcoplasmic Ca<sup>2+</sup> release in response to ISO (300 nM) followed by a caffeine test in cardiomyocytes isolated from one WT and two MKK6 KO 2-month-old mice. Relative fluorescence levels of a Ca<sup>2+</sup>-sensitive dye (Fluo-4) were used to measure relative levels of intracellular Ca<sup>2+</sup>. The red stroke arrows indicate SCR events, given by spontaneous Ca<sup>2+</sup> transients, observed in MKK6 KO cardiomyocytes.

**b**, Intracellular Ca<sup>2+</sup> handling properties of WT (twitch transient:  $n = 61$  and  $39$ ; SR fractional release:  $n = 20$  and  $37$ ; caffeine-induced transient:  $n = 20$  and  $38$ ; SCR:  $n = 31$  and  $31$ ; in basal and in response to ISO stimulation, respectively) and MKK6 KO (twitch transient:  $n = 42$  and  $24$ ; SR fractional release:  $n = 14$  and  $24$ ; caffeine-induced transient:  $n = 15$  and  $24$ ; SCR:  $n = 25$  and  $25$ ; in basal and in response to

ISO stimulation, respectively) cardiomyocytes in the presence and absence of ISO. MKK6 KO cardiomyocytes showed impaired Ca<sup>2+</sup> transient ISO response and increased frequency of SCR.  $\Delta F/F_0$  = change of fluorescence intensity relative to baseline; F/F<sub>0</sub> = fluorescence intensities relative to baseline. Data were collected from three independent myocyte isolations for each condition. Two-sided Fisher's exact test was used to compare proportions (**b** rightward lower panel). Two-way ANOVA followed by Sidak's post test was used to compare differences between genotypes (**b** top and leftward lower panels). **c**, Immunoblot analysis of the phosphorylation and protein levels of SERCA2 and PLN in ventricles from 2-month-old WT ( $n = 4$ ) and MKK6 KO ( $n = 5$ ) male mice. Two-sided unpaired Student's *t*-test. Data are expressed as mean  $\pm$  s.e.m.

and reduced localization of Kv4.3 channel at the plasma membrane. This was concomitant with SR Ca<sup>2+</sup> leak, APD prolongation and stress-triggered arrhythmias.

Knowledge about the underlying mechanisms that link aging with increased susceptibility to cardiac arrhythmogenesis is limited. In the ventricles, the substrate for arrhythmia in the elderly will vary depending on the existence of previous structural heart disease<sup>5</sup>. Cardiac fibrosis is known to be increased during aging and

to alter cardiac conduction, promoting arrhythmias<sup>43,44</sup>. However, the susceptibility to ventricular arrhythmogenesis is enhanced in the aged heart even without evident structural abnormalities<sup>5,45,46</sup>, indicating that additional mechanisms act to promote arrhythmogenesis. Notably, we used p38 $\gamma/\delta$  activation mouse models with normal cardiac function and no fibrosis<sup>11,47</sup> to avoid the participation of other mechanisms involved in the development of ventricular arrhythmia.



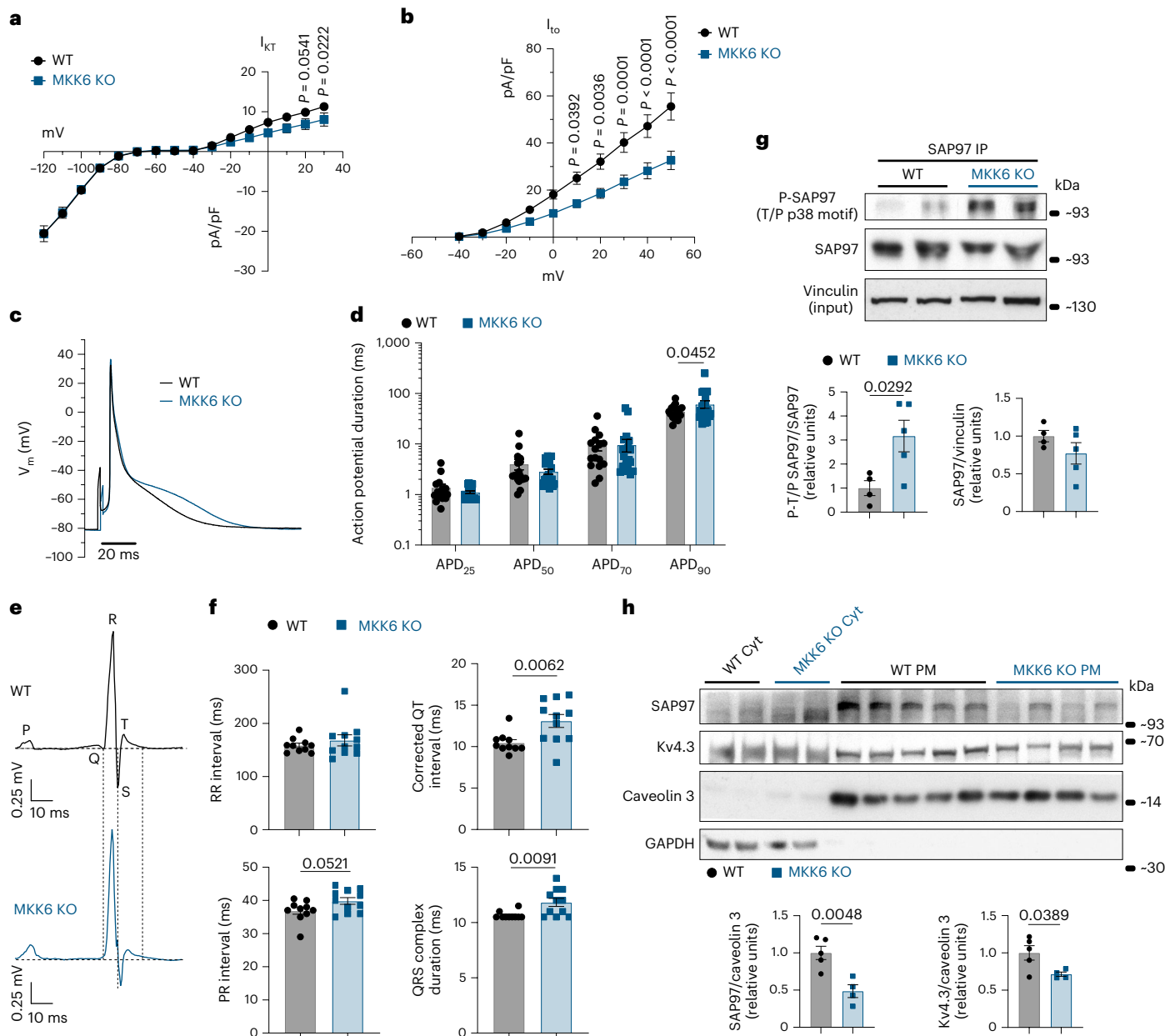


**Fig. 6 | Transient outward potassium current is reduced, and APD and QT interval are prolonged, in MKK6 KO mice. a**, Total potassium current ( $I_{KT}$ ) I/V relationship in cardiomyocytes from 2-month-old WT ( $n = 15$ ) and MKK6 KO ( $n = 10$ ) mice. Mean peak current densities at  $-120$  mV were  $-20 \pm 1.8$  (WT) versus  $-20 \pm 0.7$  (MKK6 KO) pA/pF. Each point was measured at steady state (end of the voltage pulse). Two-way ANOVA followed by Sidak's post test. Data were collected from three independent myocyte isolations for each condition. **b**, Transient outward potassium current ( $I_{to}$ ) I/V relationship of the difference between beginning peak and sustained  $I_{to}$  in WT ( $n = 15$ ) and MKK6 KO ( $n = 16$ ) cardiomyocytes. Mean peak current densities at 40 mV were  $47 \pm 4$  (WT) versus  $28 \pm 3$  (MKK6 KO) pA/pF. Two-way ANOVA followed by Sidak's post test. Data were collected from three independent myocyte isolations for each condition. **c**, Superimposed APs of isolated cardiomyocytes from WT and MKK6 KO mice paced at 1 Hz. **d**, APD at 25%, 50%, 70% and 90% repolarization in WT ( $n = 16$ )

and MKK6 KO ( $n = 22$ ) cardiomyocytes. Two-way ANOVA followed by Sidak's post test. Data were collected from three independent myocyte isolations for each condition. **e, f**, Representative lead-II surface ECG of one heartbeat (**e**) and ECG intervals (**f**) in anesthetized WT ( $n = 10$ ) and MKK6 KO ( $n = 11$ ) mice. Two-sided unpaired *t*-test or Mann-Whitney *U*-test. **g**, SAP97 immunoprecipitation indicating increased phosphorylation in p38 target T/P motif in MKK6 KO mice. Immunoblot against vinculin was used as a loading control in the whole lysates. WT  $n = 4$ ; MKK6 KO  $n = 5$ . Two-sided unpaired *t*-test. **h**, Subcellular fractionation analysis of the localization of SAP97 and Kv4.3 in heart lysates from WT (cytosol  $n = 2$ ; plasma membrane  $n = 5$ ) and MKK6 KO (cytosol  $n = 2$ ; plasma membrane  $n = 4$ ) mice. Caveolin 3 was used as plasma membrane loading control, and GAPDH was used as cytosol loading control. Cyt, cytosol; PM, plasma membrane. Two-sided unpaired *t*-test. Data are mean  $\pm$  s.e.m. IP, immunoprecipitation.

It was previously shown that phosphorylation of p38 MAPK is augmented during aging in tissues such as lung or brain<sup>48</sup>. However, previous studies did not report increased p38 phosphorylation in cardiac tissue<sup>45,48</sup>. Notably, those studies also did not address the phosphorylation levels of the different p38 family members,

as we have done. Although we did not find differences in p38 $\alpha/\beta$  phosphorylation, we did demonstrate that p38 $\gamma/\delta$  were phosphorylated in ventricles during aging (Fig. 1a). Despite belonging to the same family, the different p38 MAPK members show different substrate selectivity and inhibitor susceptibility<sup>10,12</sup>, highlighting

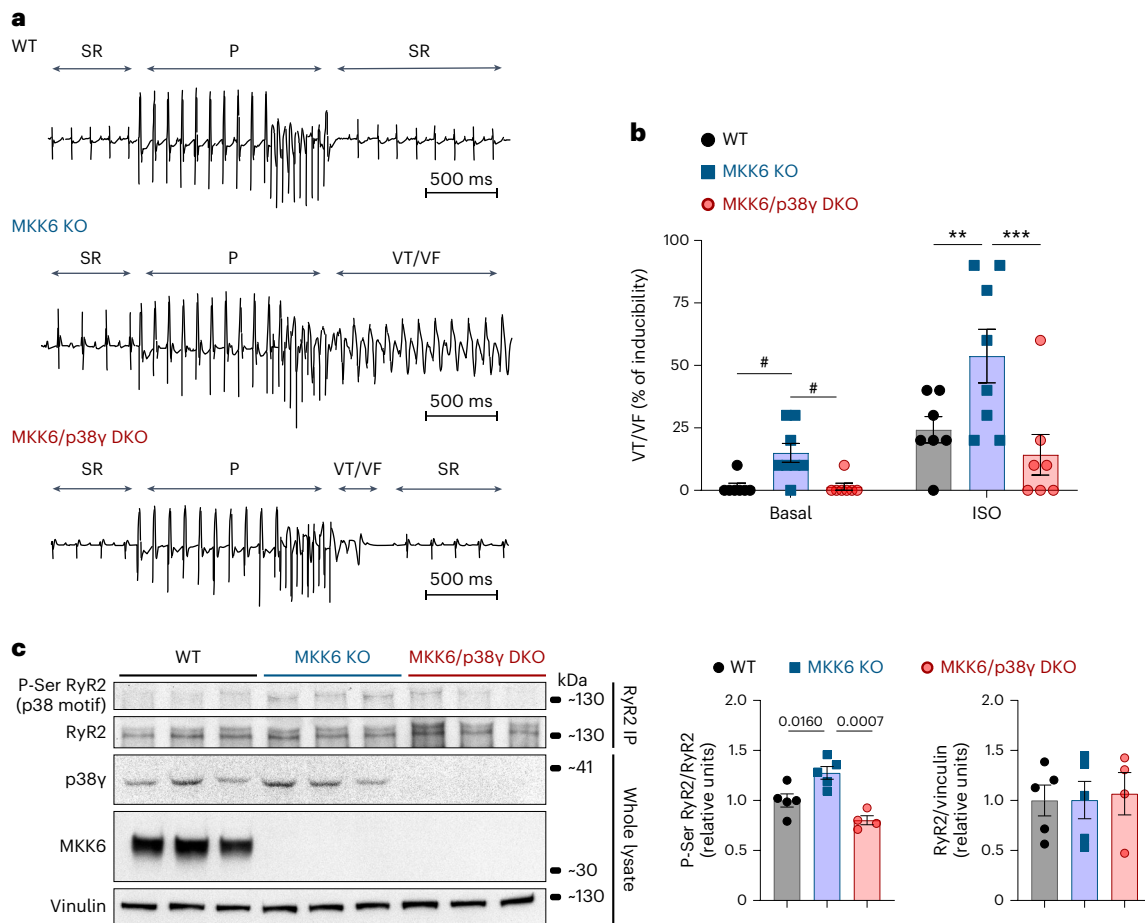


**Fig. 7 | p38 $\gamma$  deficiency reduces arrhythmia susceptibility and RyR2 phosphorylation in MKK6 KO mice.** **a**, Surface lead-II ECGs during sinus rhythm (SR) and intracardiac rapid pacing (P) in anesthetized 2-month-old WT, MKK6 KO and MKK6/p38 $\gamma$  DKO mice. After ISO administration (i.p. 5 mg kg<sup>-1</sup>), a brief train of intracardiac ventricular pacing stimuli triggered a relatively long episode of VT/VF in MKK6 KO mice, whereas WT and MKK6/p38 $\gamma$  DKO rapidly recovered the SR after the pacing stimuli. **b**, Percentage of VT/VF inducibility by S1-S2 protocol 1 in WT ( $n = 7$ ), MKK6 KO ( $n = 8$ ) and MKK6/p38 $\gamma$  DKO ( $n = 7$ ) mice in the absence

(basal) and presence (ISO) of isoproterenol. Each dot shows the percentage of VT/VF induced in each mouse by the S1-S2 protocol.  $**P = 0.0058$  and  $***P = 0.0002$ , two-way ANOVA followed by Tukey's post test;  $*P = 0.0104$  (WT versus MKK6 KO) and  $*P = 0.0104$  (MKK6 KO versus MKK6/p38 $\gamma$  DKO), Kruskal-Wallis test followed by Dunn's multiple comparisons test. **c**, Immunoblot evaluation of RyR2 phosphorylation at P-Ser p38 motif in heart lysates from 2-month-old WT ( $n = 3$ ), MKK6 KO ( $n = 3$ ) and MKK6/p38 $\gamma$  DKO ( $n = 3$ ) mice. Two-sided unpaired Student's  $t$ -test. Data are mean  $\pm$  s.e.m. IP, immunoprecipitation.

the importance of differentiating the specific action of each one of these kinases.

Another age-related change observed in the heart is mitochondrial dysfunction and reduced oxidative phosphorylation capacity<sup>49</sup>. These metabolic changes increase susceptibility to cardiac dysfunction in situations of high energy demand, for instance during tachyarrhythmias<sup>50</sup>. Interestingly, p38 $\gamma/\delta$  regulate the cardiac adaptive metabolic shift from glycolytic energy production to fatty acid oxidation during the first weeks of postnatal development<sup>21</sup>. Premature induction of p38 $\gamma/\delta$  in newborn mice reduced glycogen production and cardiomyocyte energy supply, promoting cardiac dysfunction<sup>21</sup>. Remarkably, it has been shown that glycolytic inhibition promotes ventricular arrhythmia in aged hearts<sup>51</sup>. It would be interesting to explore if there is a connection between the increased activation of p38 $\gamma/\delta$  and changes in cardiac metabolism in the aged heart, which could contribute to the higher susceptibility of the cardiomyocyte to failure under stress conditions, such as during arrhythmias at advanced ages. It is noteworthy that WPW syndrome was one of the top pathologies associated with the phosphoproteome change induced by p38 $\gamma/\delta$  activation (Fig. 2e). This syndrome leads to abnormal impulse propagation and a higher risk of ventricular arrhythmia in specific conditions, such as atrial fibrillation with adrenergic stimuli<sup>52,53</sup>. The etiology of the disease is usually

attributed to the existence of an accessory conduction pathway due to defects in cardiac embryogenesis. However, a small percentage of WPW syndromes are familial and caused by mutations in *PRKAG2*, a gene encoding for a subunit of AMPK, resulting in cardiac conduction problems due to excessive cardiac glycogen storage<sup>54</sup>. Given the role of p38 $\gamma/\delta$  in the regulation of cardiac metabolism<sup>21</sup> and that AMPK directly regulates p38 MAPK<sup>35,36</sup>, it would surely be worth a further investigation into the role of the p38 MAPK pathway in WPW syndrome.

At the molecular level, our findings show that p38 $\gamma/\delta$  phosphorylation led to increased RyR2 phosphorylation at Ser-2367. Although this site deviates from the canonical proline-directed motif, recent research suggests that p38 kinases can also target non-proline-directed sites<sup>57</sup>. To further elucidate the significance of p38 kinases in the direct phosphorylation of this residue, directed mutagenesis experiments may be warranted. Interestingly, this specific phosphorylation site was previously identified as a negative regulator of RyR2 function<sup>30</sup>. The phosphorylation at Ser-2367 may play a crucial role in the modulation of RyR2 activity and potentially contribute to the susceptibility of ventricular arrhythmias in different disease conditions. Further investigation into the functional implications of this phosphorylation event will help us better understand the complex regulatory mechanisms involving p38 $\gamma/\delta$  and their effects on RyR2

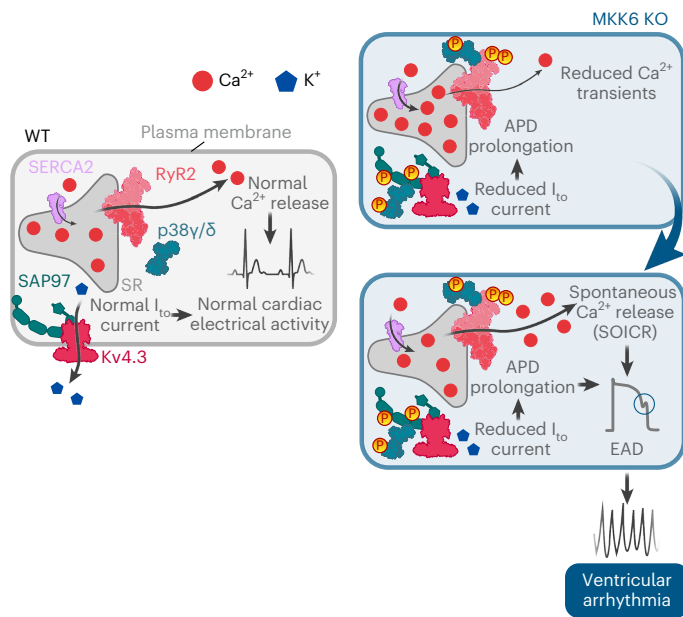


**Fig. 8 | Proposed model for ventricular arrhythmia susceptibility mediated by increased p38 $\gamma$ / $\delta$  activity.** p38 $\gamma$ / $\delta$  activation due to MKK6 deficiency leads to hyperphosphorylation of RyR2 at Ser-2367, resulting in reduced RyR2 activity and reduced calcium transients. At the same time, p38 $\gamma$ / $\delta$  activation promotes SAP97 hyperphosphorylation, promoting reduced translocation of Kv4.3 channels to the plasma membrane, which results in reduced  $I_{to}$  current and prolongation of the APD. The reduced  $Ca^{2+}$  transients, together with the APD prolongation, lead to SCR by store-overload-induced calcium release (SOICR), promoting EADs (blue circle), which eventually deteriorate in ventricular arrhythmias. The presumably increased SERCA2-mediated SR calcium reuptake also likely contributes to the SOICR in MKK6 KO cardiomyocytes.

function and cardiac pathophysiology. The reduced  $Ca^{2+}$  transients observed in our study also indicate that p38 $\gamma$ / $\delta$  phosphorylation decreases RyR2 function. This reduction in RyR2 function, along with the presence of stress signals such as stimulation plus ISO, contributes to the development of malignant arrhythmias. This pattern is similar to the effects seen in certain RyR2 mutations that have a dominant negative effect and lead to prolonged APs, spontaneous EADs and stress-induced VF<sup>31</sup>. These arrhythmic events are attributed to spontaneous SR  $Ca^{2+}$  release through a mechanism known as store-overload-induced  $Ca^{2+}$  release<sup>24,31–33</sup>. Our findings also revealed increased phosphorylation of PLN and reduced levels of PLN protein in MKK6 KO hearts. This suggests a reduction in the inhibitory control of SERCA2 activity, which likely explains the unchanged SR content despite the increased RyR2-mediated  $Ca^{2+}$  release (Fig. 5). Together with RyR2 phosphorylation, p38 $\gamma$ / $\delta$  hyperphosphorylation also resulted in increased SAP97 phosphorylation, altered Kv4.3 localization and reduced  $I_{to}$ . The prolonged AP resulting from reduced  $I_{to}$  current leads to a longer depolarization period, allowing for a higher net influx of calcium through the L-type calcium channel and impairing calcium removal via the  $Na^+/Ca^{2+}$  exchanger. As a result, calcium accumulation within the cell occurs<sup>58</sup>. Together with increased SERCA2-mediated SR  $Ca^{2+}$  uptake and reduced RyR2 function due to p38 $\gamma$ / $\delta$  phosphorylation, these mechanisms likely contribute to store-overload-induced  $Ca^{2+}$  release and increased susceptibility to ventricular arrhythmias in MKK6 KO mice (Fig. 8).

Notably, our results are in line with previous evidence reporting that cardiac-specific ablation, or expression of genetic variants of SAP97, alters the cardiac electrophysiological properties, specifically  $I_{to}$ , APD and QT interval<sup>59–61</sup>, and mutations in SAP97 have been proposed as a pathogenic substrate for Brugada syndrome<sup>61</sup>.

Our results support a critical role of p38 $\gamma$ / $\delta$  in the control of cardiac electrophysiology and the promotion of ventricular arrhythmia. We specifically addressed the role of these p38 family members in cardiac arrhythmia, highlighting p38 $\gamma$ / $\delta$  inhibition as an interesting and still unexplored therapeutic strategy. Deletion of p38 $\gamma$  protected MKK6 KO from VF development and reduced the duration of the arrhythmia in aged p38 $\gamma$  KO mice. However, p38 $\gamma$  KO mice did not show a reduced susceptibility to cardiac arrhythmia compared with WT mice. These findings suggest that, although blocking the p38 pathway may provide partial protection against VF in age-related cardiac arrhythmias, it is important to note that age-related cardiac arrhythmias are complex and multifactorial, involving various remodeling processes and signaling pathways. For example, previous research highlighted the involvement of cardiomyocyte remodeling, activation of JNK and gap junction remodeling in age-related cardiac arrhythmias<sup>14,62,63</sup>. These additional pathways and mechanisms may contribute to the development of arrhythmias in aged animals independently of p38 $\gamma$ / $\delta$  signaling. The inhibition of p38 has been explored therapeutically for the treatment of several diseases, including cancer and CVDs. However, most p38 inhibitors target p38 $\alpha$ / $\beta$  family members but not p38 $\gamma$ / $\delta$  or are non-specific and inhibit all p38 family members. Furthermore, results from clinical trials using inhibitors of p38 $\alpha$ / $\beta$  have been disappointing<sup>10</sup>. Our work underscores the current need for the pharmacological development of specific p38 $\gamma$ / $\delta$  inhibitors for further investigation of this pathway as a target for anti-arrhythmic therapy.

## Methods

### Animal preparation

MKK6 KO mice (B6.129-*Map2k6*<sup>tm1Flv</sup>) were as previously described<sup>64</sup>. The p38 $\gamma$ -negative line (B6.129-*Mapk12*<sup>tm1</sup>)<sup>41</sup> was crossed with the MKK6 KO line (B6.129-*Map2k6*<sup>tm1Flv</sup>) to generate the double knockout (DKO) mice (MKK6/p38 $\gamma$  DKO). Mice were backcrossed for 10 generations or more to the C57BL/6J background. The sex and age of the mice for each experiment are specified in each figure legend. The genotype was confirmed by polymerase chain reaction (PCR) analysis of genomic DNA. For signaling studies, animals were killed by cervical dislocation.

All animal procedures were approved by the Centro Nacional de Investigaciones Cardiovasculares (CNIC) Ethics Committee and the Madrid regional authorities (ref. PROEX 215/18) and conformed to EU Directive 86/609/EEC and Recommendation 2007/526/EC regarding the protection of animals used for experimental and other scientific purposes, enacted under Spanish law Real Decreto 53/2013.

### Adenoviral vector production and administration

AAV plasmids were cloned and propagated in the Stb13 *Escherichia coli* strain (Life Technologies). Shuttle plasmids pCEFL Flag p38 $\gamma$  D129A, pCMV Flag p38 $\delta$  F324S and pAAV-GFP were derived from the pAcTnT plasmid to generate pAAV-TnT-p38 $\gamma$ <sub>act</sub>, pAAV-TnT-p38 $\delta$ <sub>act</sub> and pAAV-TnT-GFP-Luc, respectively. These AAV plasmids were packaged into AAV-9 capsids with the use of pAdDF6 helper plasmids (providing the three adenoviral helper genes) and pAAV2/9 (providing rep and cap viral genes), obtained from the Penn Vector Core. Shuttle vectors were generated by direct cloning (GeneScript) of synthesized NheI-SalI fragments into pAcTnT cut with the same restriction enzymes.

The AAV shuttle and helper plasmids were transfected into HEK293A cells by calcium phosphate co-precipitation. A total of 840  $\mu$ g of plasmid DNA (mixed in an equimolar ratio) was used per HYPERFlask (Corning) seeded with  $1.2 \times 10^8$  cells the day before. Seventy-two hours after transfection, the cells were collected by centrifugation, and the cell pellet was resuspended in TMS (50 mM Tris HCl, 150 mM NaCl, 2 mM  $MgCl_2$ ) on ice before digestion with DNase I and RNase A (0.1 mg ml<sup>-1</sup> each, Roche) at 37 °C for 60 min. Clarified supernatant containing the viral particles was obtained by iodixanol gradient centrifugation<sup>65</sup>. Gradient fractions containing the viruses were concentrated using Amicon UltraCel columns (Millipore) and stored at -70 °C. A total of  $10^{11}$



viral particles (diluted in PBS) per mouse were injected intravenously through the tail vein. Mice were injected at 7 weeks of age and killed for analysis 2 weeks after the injection.

### Immunoblot analysis

Tissue extracts were prepared in Triton or CHAPS lysis buffer (20 mM Tris (pH 7.4), 1% Triton X-100 or 0.1% CHAPS, 10% glycerol, 137 mM NaCl, 2 mM EDTA, 25 mM  $\beta$ -glycerophosphate, 1 mM sodium orthovanadate, 1 mM phenylmethylsulfonyl fluoride and 10  $\mu$ g ml<sup>-1</sup> aprotinin and leupeptin). For isolation of plasma membrane fraction, the hearts were homogenized in HES buffer (20 mM HEPES, 1 mM EDTA, 250 mM sucrose, pH 7.4) with protease and phosphatase inhibitors. The lysate was then centrifuged at 500g, 10 min, 4 °C, and the supernatant was transferred into new tubes followed by centrifugation at 10,800g, 12 min, 4 °C. The supernatant (cytosol) was transferred into new tubes, and the pellet (plasma membrane) was dissolved in CHAPS lysis buffer. Extracts (20–50  $\mu$ g of protein) and immunoprecipitates (prepared from 0.5–3 mg) were examined by immunoblot. For immunoprecipitation assays, heart extracts were incubated with 1–4  $\mu$ g of the specific antibody coupled to Protein G Sepharose (GE Healthcare). After incubation overnight at 4 °C with agitation, the captured proteins were centrifuged at 10,000g; the supernatants were collected; and the beads were washed four times in PBS 1 $\times$ . Beads were boiled for 5 min at 95 °C in 10  $\mu$ l of sample buffer. Extracts and immunoprecipitates were examined by SDS–PAGE and blotted with antibodies to the following targets: SAP97 (DU391) (MRC PPU) at 1  $\mu$ g ml<sup>-1</sup>; vinculin (Sigma-Aldrich) at 1:5,000 dilution; MKK6 (9264S), phospho-p38 MAPK (Thr180/Tyr182) (9211S), phospho-MAPK/CDK substrates (34B2) (2325S), phospho-threonine-proline (P-Thr-Pro-101) (9391S), p38 $\gamma$  MAPK (2307S), phospho-phospholamban (Ser16/Thr17) (8496) (Cell Signaling Technology); RyR (F-1) (sc-376507), p38 $\alpha$  (C-20) (sc-535-G), SERCA2 (IID8) (sc-53010) and GAPDH (FL-335) (sc-25778) (Santa Cruz Biotechnology); RyR2 (C3-33) (MA3-916) and phospho-p38 MAPK gamma/delta (Tyr185, Tyr182) (PA5-105907) (Thermo Fisher Scientific); Kv4.3 (75-017) (NeuroMab); and Caveolin 3 (610420) (BD Biosciences), all at 1:1,000 dilution. Phosph-PLN (Thr 17) (A010-13) and PLN (A010-14) from Badrilla were at 1:5,000 dilution. Immunocomplexes were detected by enhanced chemiluminescence (GE Healthcare Life Sciences). Immunoblots were quantified using ImageJ software<sup>66</sup>.

### hiPSC-derived cardiomyocytes

Cardiomyocyte lineage differentiation of WT hiPSC line HDF-iPS-SV10 (Spanish National Stem Cell Bank, ISCIII) was achieved using small molecules, CHIR99021 and IWP4, as previously described<sup>67</sup>. In brief, hiPSCs were maintained on a Matrigel-coated cell culture dish in Essential 8 medium, at 37 °C, 5% CO<sub>2</sub>, changing the medium daily. hiPSCs were dissociated with 0.5 mM EDTA when 70–90% confluence was reached (usually 5 d after passaging). hiPSCs were seeded in a new Matrigel dish. On day 0 of differentiation, Essential 8 medium was changed to RPMI/B27 without insulin (RPMI/B27minus) containing GSK3 inhibitor (CHIR99021). Exactly 24 h later, CHIR99021 was withdrawn, and cells were maintained in RPMI/B27minus. On day 3 of differentiation, IWP4 inhibitor was added, and it was withdrawn at day 5. From day 7 of differentiation, cells were maintained in culture with RPMI/B27 plus insulin, changing the medium every 3 d. At day 9–12 of differentiation, cells presented spontaneously beating phenotype. Once differentiated, hiPSC-derived cardiomyocytes were treated with or without isoproterenol 1  $\mu$ M for 30 min before being processed for immunoblot analysis.

### Kinase assay

For the in vitro phosphorylation assay of RyR2, the plasma membrane fraction was isolated from heart lysates of WT mice as described above. The plasma membrane fraction was immunoprecipitated with RyR2 antibody as described above. Isolated RyR2 was then incubated with recombinant active p38 $\alpha$  (SAPK2a (p38 alpha) (1–360)\* DU979, MRC

PPU), p38 $\beta$  (SAPK2b (p38 beta) (1–364)\* DU1791, MRC PPU), p38 $\gamma$  (SAPK3 (p38 gamma) (1–367)\* DU980, MRC PPU), p38 $\delta$  (SAPK4 (p38 delta) (1–365)\* DU981, MRC PPU) or p38 $\gamma$  and  $\delta$  (0.1 U of each kinase) in kinase buffer (50 mM Tris-HCl, pH 7.5, 0.1% 2-mercaptoethanol, 0.1 mM EGTA, 0.1 mM sodium vanadate, 10 mM magnesium acetate) or with kinase buffer alone. Then, 100  $\mu$ M ATP was added to each reaction and incubated at 30 °C for 30 min. Each reaction was stopped and tested for immunoblot as described above.

### ECG analysis

Data were stored for offline analysis using custom scripts in MATLAB for pre-processing, visualization and quantification of electrophysiological intervals and heart rate variability. After band-pass filtering between 0.5 Hz and 200 Hz, baseline wander was removed using a bidirectional filtering strategy. ECG segments with noise artifacts were manually removed and excluded for further analysis. Parabolic fitting of the coillet wavelet transformation and further detection of the maximum magnitude point was used to detect the R-peak of the QRS complex. All R-peak detections were supervised to ensure the accuracy of ECG segmentations. After QRS complex and P and T wave detection, ECG intervals were extracted using adaptive windowing depending upon beat-to-beat RR changes. Specifically: (1) PR intervals were measured from the beginning of the P wave to the beginning of the R wave/Q wave; (2) QRS intervals were measured from the beginning of the Q wave until the point where the S wave crosses the baseline; and (3) QT intervals were measured from the beginning of the Q wave until the point where the T wave declines to 90% (T90) from the peak<sup>68</sup>. Adaptive heart-rate-corrected QT values (QTc) were derived using a modification of Bazette's formula for murine electrocardiography<sup>69</sup>.

### Isolation of murine cardiac myocytes

Mice cardiac myocytes were isolated using the standard Langendorff technique. Calcium-tolerant free wall left ventricular cardiomyocytes were isolated from the hearts of WT or MKK6 KO age-matched mice as previously described<sup>70,71</sup>. In brief, mice were intraperitoneally (i.p.) injected with 1 ml of heparin (100 IU ml<sup>-1</sup>) 20 min before heart excision. Animals were anesthetized with 2% isoflurane, and the heart was removed quickly from the chest and retrogradely perfused through the aorta at a constant flow (4 ml min<sup>-1</sup>) at 37 °C for 4 min with a Ca<sup>2+</sup>-free buffer containing (in mmol L<sup>-1</sup>) 113 NaCl, 4.7 KCl, 1.2 MgSO<sub>4</sub>, 0.6 Na<sub>2</sub>HPO<sub>4</sub>, 0.6 KH<sub>2</sub>PO<sub>4</sub>, 10 KHCO<sub>3</sub>, 12 NaHCO<sub>3</sub>, 10 HEPES, 10 2,3-butanedione monoxime (BDM, Sigma-Aldrich), 30 taurine and 5.5 glucose. All solutions were filtered (0.2- $\mu$ m filter) and equilibrated with 100% O<sub>2</sub> for at least 20 min before use. Enzymatic digestion was initiated by adding collagenase type II (773.4 U ml<sup>-1</sup>, Worthington), trypsin (0.14 mg ml<sup>-1</sup>) and CaCl<sub>2</sub> (12.5  $\mu$ mol L<sup>-1</sup>) to the perfusion solution. After 5–8 min of digestion, the free wall of the left ventricle was removed, and single cells were isolated by physical separation. Cells were used for electrophysiological recordings within 8 h after isolation.

### Electrophysiology in mice free wall left ventricular cardiomyocytes

During experiments and data analysis, electrophysiological scientists were blinded to the experimental phenotype of mice. Experiments were carried out using a Multiclamp 700B amplifier (Molecular Devices). Data were acquired and analyzed using pCLAMP 10 (Molecular Devices). Borosilicate glass electrodes were pulled with a Brown–Flaming puller (model P-97), yielding appropriate tip resistances when filled with pipette solution to enable proper voltage control.

**APs.** APs were elicited using square wave pulses (30–50-pA amplitude, 5–8-ms duration), generated by a DS8000 digital stimulator (World Precision Instruments) and recorded at 37 °C with pipette solution containing (in mmol L<sup>-1</sup>) 1 MgCl<sub>2</sub>, 1 EGTA, 150 KCl, 5 HEPES, 5 phosphocreatine, 4.46 K<sub>2</sub>ATP and 2  $\beta$ -hydroxybutyric acid, pH adjusted to 7.2



with KOH, with pipette resistance of 4–6 M $\Omega$ . Extracellular solution contained (in mmol L<sup>-1</sup>) 148 NaCl, 0.4 NaH<sub>2</sub>PO<sub>4</sub>, 1 MgCl<sub>2</sub>, 5.5 glucose, 5.4 KCl, 1 CaCl<sub>2</sub>, 15 HEPES and 1 EGTA, pH adjusted to 7.4 with NaOH. AP properties, including resting membrane potential (RMP), overshoot, AP amplitude and AP duration 25%, 50%, 70% and 90% of repolarization, were analyzed using custom-made software developed by Krzysztof Grzeda for the Center of Arrhythmia Research at the University of Michigan. Maximum upstroke velocity  $dV/dt_{max}$  was estimated using OriginPro 9 (OriginLab Corporation).

All ion currents were recorded at room temperature (20–22 °C) with pipette resistance between 1.5 M $\Omega$  and 3 M $\Omega$ .

**I<sub>Na</sub> sodium current in mouse cardiomyocytes.** Pipette filling solution (in mmol L<sup>-1</sup>): 5 NaCl, 60 CsF, 10 EGTA, 5 MgATP, 75 choline chloride and 5 HEPES, pH 7.2. The extracellular solution contained (in mmol L<sup>-1</sup>) 5 NaCl, 1 MgCl<sub>2</sub>, 1.8 CaCl<sub>2</sub>, 0.1 CdCl<sub>2</sub>, 11 glucose, 60 CsCl, 72.5 choline chloride and 20 HEPES, pH 7.35. Appropriate whole-cell capacitance and series resistance compensation ( $\geq 70\%$ ) was applied, along with leak subtraction using a P/4 protocol. To assess the I<sub>Na</sub> density, cells were held at -160 mV and stepped to various test potentials (-80 mV to 60 mV in 5-mV or 10-mV increments, 200-ms duration and 2,800-ms inter-pulse intervals).

**L-type calcium current (I<sub>CaL</sub>) in mouse cardiomyocytes.** Pipette filling solution (in mmol L<sup>-1</sup>): 120 CsCl, 20 TEA-Cl, 1 MgCl<sub>2</sub>, 5 MgATP, 0.2 Na<sub>2</sub>GTP, 10 HEPES and 10 EGTA, pH adjusted to 7.2 with CsOH. External solution (in mmol L<sup>-1</sup>): 137 NaCl, 5.4 CsCl, 1 MgCl<sub>2</sub>, 1 CaCl<sub>2</sub>, 10 HEPES, 10 glucose, 2,4-aminopyridine (4-AP) and 10  $\mu$ mol tetrodotoxin (TTX), pH adjusted to 7.4 with NaOH.

Voltage dependence of peak I<sub>CaL</sub> was measured by holding at -50 mV, and 300-ms voltage steps were applied from -50 mV to +60 mV in 10-mV increments.

**Inward rectifier potassium current (I<sub>K1</sub>) in mouse cardiomyocytes.** Pipette filling solution (in mmol L<sup>-1</sup>): 150 KCl, 1 MgCl<sub>2</sub>, 5 EGTA, 5 HEPES, 5 phosphocreatine, 4.4 K<sub>2</sub>ATP and 2  $\beta$ -hydroxybutyric acid, pH 7.2. The standard external solutions contained (in mmol L<sup>-1</sup>): 148 NaCl, 0.4 NaH<sub>2</sub>PO<sub>4</sub>, 1 MgCl<sub>2</sub>, 5.4 KCl, 1.8 CaCl<sub>2</sub>, 5.5 glucose and 15 HEPES, pH 7.4. For I<sub>K1</sub> measurements, 5  $\mu$ mol L<sup>-1</sup> nifedipine was added to block I<sub>CaL</sub>, and 1 BaCl<sub>2</sub> mmol L<sup>-1</sup> was used to isolate I<sub>K1</sub> from other background currents.

I<sub>K1</sub> was recorded using a step protocol from a holding potential of -50 mV and stepping from -120 mV to +30 mV in 10-mV increments of 500-ms duration at each potential.

**Transient outward potassium current (I<sub>to</sub>) in mouse cardiomyocytes.** Pipette filling solution (in mmol L<sup>-1</sup>): 150 KCl, 1 MgCl<sub>2</sub>, 5 EGTA, 5 HEPES, 5 phosphocreatine, 4.4 K<sub>2</sub>ATP and 2  $\beta$ -hydroxybutyric acid, pH adjusted to 7.2 with KOH. External solution (in mmol L<sup>-1</sup>): 148 NaCl, 0.4 NaH<sub>2</sub>PO<sub>4</sub>, 1 MgCl<sub>2</sub>, 5.5 glucose, 5.4 KCl, 1 CaCl<sub>2</sub> and 15 HEPES, pH adjusted to 7.4 with NaOH. To block sodium channels, 10  $\mu$ mol L<sup>-1</sup> TTX and 5  $\mu$ mol L<sup>-1</sup> nifedipine were added to the external solution to block calcium channels.

Potassium currents were recorded using 5-s depolarizing pulses to potentials between -40 mV and +50 mV from a holding of -70 mV. Voltage steps were in steps of 10 mV at 15-s intervals.

### ECG and intracardiac electrophysiology studies

Ventricular arrhythmia propensity was determined in anesthetized (2% isoflurane in 0.5 L min<sup>-1</sup> 100% O<sub>2</sub>) adult mice as previously described<sup>72</sup>. During continuous recording of ECG (lead II), a 1.1-Fr. octopolar stimulation-recording catheter (FTS-1113A-0518, Scisense) was inserted through the jugular vein and advanced into the right atrium, AV ring and ventricle. We ensured that the ventricular electrogram was the largest signal on the octopolar catheter and that stimulation

at low frequency activated the ventricles directly. Electrical pacing was delivered to the ventricles at twice threshold of capturing. Vulnerability to cardiac arrhythmia was assessed by delivering two different trains (S1-S2) of 10 pulses each at 10 Hz (CL = 100 ms) and 25 Hz (CL = 40 ms), respectively (S1-S2 protocol 1). Alternatively, vulnerability to cardiac arrhythmia was assessed by delivering a train pulse of fixed cycle length (CL = 100 ms) (S1) followed by a single pulse (S2) of a shorter duration. During each train, S2 was progressively reduced every 2 ms from 40 ms to 20 ms (S1-S2 protocol 2). VT/VF was assessed 10 times in basal conditions and 10 times after ISO (i.p. 5 mg kg<sup>-1</sup>) stimulation in each mouse and for each protocol.

VT/VF was defined as an excessively fast monomorphic/polymorphic ventricular rhythm independent of atrial excitation.

### Optical mapping

The heart was rapidly excised through thoracotomy, connected to a Langendorff perfusion system, perfused with warm oxygenated Tyrode's solution as described previously<sup>24–26</sup> and allowed to equilibrate for 10 min. We used the voltage-sensitive dye Di-4-ANEPPS (excitation light, 530 nm) and a CCD camera (Little Joe, 80  $\times$  80 pixels; spatiotemporal resolution 109  $\mu$ m, 600 f/s) and mapped the epicardial anterior surfaces of both ventricles. Further details were presented previously<sup>70,71</sup>. Here, 7  $\mu$ M blebbistatin was used to prevent contraction. Twelve 8–11-month-old WT and 17 MKK6 KO hearts were initially perfused with 4 mM [K<sup>+</sup>]<sub>o</sub> Tyrode's solution, followed by 4 mM Tyrode's solution containing ISO (300 nM) and high Ca (2.5 mM). Burst pacing was done using an octapolar mouse catheter (1.1 Fr) introduced through the right atria and contacting with the endocardial surface on the apex of the right ventricle, and movies were recorded from the anterior surface of the heart in the horizontal configuration. Phase maps were constructed as described previously<sup>28</sup>.

**Generation of phase movies.** Phase movies were generated by Hilbert transformation. The instantaneous phase of the AP recorded at each pixel was determined by transforming the original time-series fluorescence signals such that every spectral component was shifted by its corresponding quarter cycle. Afterward, the instantaneous phase of the signal was obtained from the inverse tangent of the ratio of the transformed signal to the original signal. The phase angle, with values between  $-\pi$  and  $+\pi$  radians, is represented as a continuous color scheme to construct a phase map, in which the continuous spatial phase change reflects the process of excitation, repolarization and recovery<sup>73–75</sup>.

### Phosphoproteomics analysis

**Sample preparation and protein digestion.** Frozen hearts were homogenized in lysis buffer comprising 100 mM Tris-HCl, pH 7.8, 4% SDS, 10 mM TCEP and phosphatase inhibitors (PhosSTOP, Roche Applied Science) using FastPrep green tubes (three times for 40 s at speed 6.0 m s<sup>-1</sup> with 1-min cooling between each run). After clarification, protein concentration in the supernatant was measured using the RC DC protein assay kit (Bio-Rad), and about 0.15 mg of proteins for each sample was subjected to FASP protocol as described previously<sup>76</sup>. In brief, protein extracts were diluted in 7 M urea in 0.1 M Tris-HCl (pH 8.5) (UA) and loaded onto 10-kDa centrifugal filter devices (Nanosep 10k Omega, Pall Life Sciences). Proteins were then alkylated with 50 mM iodoacetamide (IAA) in UA for 30 min in the dark and washed three times with UA and three times with 50 mM ammonium bicarbonate. Proteins were digested at 37 °C overnight with modified trypsin (Promega) in 50 mM ammonium bicarbonate at a 30:1 protein:trypsin (w/w) ratio. The resulting peptides were eluted with 50 mM ammonium bicarbonate and 0.5 M sodium chloride. Trifluoroacetic acid (TFA) was added to a final concentration of 1%, and the peptides were desalted onto Oasis-HLB (Waters) cartridges and dried down for further analysis.

**Isobaric labeling.** For stable isobaric labeling, the resulting tryptic peptides were dissolved in 150 mM triethylammonium bicarbonate (TEAB) buffer, and the peptide concentration was determined by measuring amide bonds with the Direct Detect system (Millipore). Equal amounts of each peptide sample were labeled using 11-plex TMT reagents (Thermo Fisher Scientific) according to the manufacturer's protocol with minor changes. Peptides were labeled with 0.8 mg of TMT reagents previously reconstituted with 70  $\mu$ l of acetonitrile, and, after incubation at room temperature for 1 h, the reaction was stopped with 0.5% TFA. After 10-min incubation, all the labeled peptide samples were pooled together. Samples were concentrated in a SpeedVac, desalted onto Oasis-HLB cartridges and dried down for further analysis. An aliquot of this mixture was separated for the analysis of the full proteome and fractionated by high-pH reverse-phase chromatography (High pH Reversed-Phase Peptide Fractionation Kit, Pierce) and dried down for further analysis.

**Phosphopeptide enrichment.** The remaining TMT-labeled sample was subjected to phosphopeptide enrichment using Ti<sup>4+</sup>-IMAC HP micro-particles (Resyn Biosciences). The magnetic particles were equilibrated with loading/binding solvent (5% TFA/0.1 M glycolic acid in 80% acetonitrile) for 5 min and incubated with the reconstituted TMT-labeled sample for 20 min. After consecutive washes with 80% ACN/1% TFA and 10% ACN/0.2% TFA, phosphopeptides were eluted with 1% ammonium hydroxide, acidified with TFA, desalted onto C18 microspin columns (The Nest Group) and dried to completion in a vacuum centrifuge. A fraction of the enriched phosphopeptides was fractionated by high-pH reverse-phase chromatography as before.

**Mass spectrometry analysis.** Labeled peptides were analyzed by liquid chromatography with tandem mass spectrometry (LC-MS/MS) using a C-18 reverse-phase nano-column (75  $\mu$ m I.D.  $\times$  50 cm, 2- $\mu$ m particle size, Acclaim PepMap RSLC, 100 C18, Thermo Fisher Scientific) in a continuous acetonitrile gradient consisting of 0–30% B in 360 min and 50–90% B in 3 min (A = 0.1% formic acid; B = 90% acetonitrile, 0.1% formic acid) at 50 °C. A flow rate of 200 nl min<sup>-1</sup> was used to elute peptides from the nano-column to an emitter nanospray needle for real-time ionization and peptide fragmentation on a Q Exactive HF Orbitrap mass spectrometer (Thermo Fisher Scientific). An enhanced FT-resolution spectrum (resolution = 70,000) followed by the MS/MS spectra from the 15th most intense parent ions were analyzed along the chromatographic run. Dynamic exclusion was set at 40 s.

**Peptide identification and quantification.** For peptide identification, all spectra were analyzed with Proteome Discoverer (version 2.1.0.81, Thermo Fisher Scientific) using SEQUEST-HT (Thermo Fisher Scientific). For database searching against the UniProt database containing all sequences from mouse and frequently observed contaminants (UniProt\_Sept20, 2018; 53,780 entries), the parameters were selected as follows: trypsin digestion with two maximum missed cleavage sites; precursor and fragment mass tolerances of 2 Da and 0.02 Da, respectively; carbamidomethyl cysteine and TMT modifications at N-terminal and Lys residues as fixed modifications; and methionine oxidation and phosphorylation of Ser, Thr and Tyr residues selected as dynamic modifications. Peptide identification was performed using the probability ratio method<sup>77</sup>, and false discovery rate (FDR) was calculated using inverted databases and the refined method<sup>78</sup> with an additional filtering for precursor mass tolerance of 15 ppm<sup>79</sup>. Identified peptides had an FDR equal to or lower than 1%. Analysis of changes in peptide abundance was performed using the quantitative information from TMT reporter intensities. The data were analysed using the iSanXoT package<sup>80,81</sup>, which applies a statistical model developed in our laboratory, which has been demonstrated to accurately describe the quantitative behavior of post-translationally modified peptides in relation to the proteins that they come from<sup>23</sup>. The algorithm is based on the

WSPP model and the Generic Integration Algorithm<sup>82,83</sup> and models the dispersion of peptide values when they are integrated to their proteins, detecting peptidofoms that significantly deviate from the expected behavior, independently from protein abundance changes. In this model, peptide log<sub>2</sub> ratios are expressed as standardized units according to their estimated variances (Z values). Differences in protein and peptide abundance were estimated based on the comparison of the groups' Zq or Zp medians, respectively. Those protein or peptide changes were considered statistically significant with  $P < 0.05$  based on limma<sup>84</sup> two-sided *t*-test comparison of the Z values. The sequence localization of phosphosites from proteins in the phosphoproteome was assigned using custom R scripts consulting PhosphoSitePlus (version 6.6.0.4.)<sup>85</sup>.

All phosphoproteomics data showing the phosphorylation site and expression Z values, along with the limma P values, can be found in Supplementary Tables 4 and 8.

The mass spectrometry proteomics data have been deposited to the ProteomeXchange Consortium via the PRIDE<sup>86</sup> partner repository with the dataset identifier PXD045996.

### Bioinformatics analysis

The phosphoproteomics dataset, which included UniProt identifiers, Z value differences of the phosphopeptides identified and P values of the Z values comparison from limma, was submitted into IPA<sup>22</sup> for core analysis with a cutoff of phosphorylation Z value difference  $> 0$  and limma two-sided *t*-test  $P < 0.05$ . Only phosphopeptides were considered for the analysis. Significantly enriched (two-sided Fisher's exact test  $P < 0.05$ ) Tox Functions and the proteins involved were identified using IPA. The network of proteins was constructed using stringApp<sup>87</sup> and Omics Visualizer<sup>88</sup> within the Cytoscape software<sup>89</sup>.

### Statistical analysis

Results are expressed as mean  $\pm$  s.e.m. A difference of  $P < 0.05$  was considered significant. Gaussian (normal) distribution was determined using the Shapiro–Wilk normality test, examination of Q–Q plots and visual examination of the population distribution. For normally distributed populations, differences between groups were examined for statistical significance by two-tailed Student's *t*-test (two groups) and one-way ANOVA followed by Tukey's post test (three or more groups). To test the respective roles of treatment and genotype, a two-way ANOVA was performed. Sidak's post test or Tukey's post test was subsequently employed when appropriate. For data that failed normality testing, Mann–Whitney *U*-test (two groups) or Kruskal–Wallis test followed by Dunn's multiple comparisons test (three groups) was performed. Two-sided Fisher's exact test was used to compare proportions.

### Reporting summary

Further information on research design is available in the Nature Portfolio Reporting Summary linked to this article.

### Data availability

All data supporting the findings of this study are included in the main article and associated files. Uncropped immunoblots are provided as Source Data. The mass spectrometry proteomics data have been deposited to the ProteomeXchange Consortium via the PRIDE<sup>86</sup> partner repository with the dataset identifier PXD045996.

### References

1. Srinivasan, N. T. & Schilling, R. J. Sudden cardiac death and arrhythmias. *Arrhythm. Electrophysiol. Rev.* **7**, 111–117 (2018).
2. Adabag, A. S., Luepker, R. V., Roger, V. L. & Gersh, B. J. Sudden cardiac death: epidemiology and risk factors. *Nat. Rev. Cardiol.* **7**, 216–225 (2010).

3. Virani, S. S. et al. Heart disease and stroke statistics—2021 update. *Circulation* **143**, E254–E743 (2021).
4. Huikuri, H. V., Castellanos, A. & Myerburg, R. J. Sudden death due to cardiac arrhythmias. *N. Engl. J. Med.* **345**, 1473–1482 (2001).
5. Mirza, M., Strunets, A., Shen, W. K. & Jahangir, A. Mechanisms of arrhythmias and conduction disorders in older adults. *Clin. Geriatr. Med.* **28**, 555–573 (2012).
6. Hatch, F., Lancaster, M. K. & Jones, S. A. Aging is a primary risk factor for cardiac arrhythmias: disruption of intracellular Ca<sup>2+</sup> regulation as a key suspect. *Expert Rev. Cardiovasc. Ther.* **9**, 1059–1067 (2011).
7. Tanaka, Y. et al. Trends in cardiovascular mortality related to atrial fibrillation in the United States, 2011 to 2018. *J. Am. Heart Assoc.* **10**, 20163 (2021).
8. Zimetbaum, P. Antiarrhythmic drug therapy for atrial fibrillation. *Circulation* **125**, 381–389 (2012).
9. Nikolic, I., Leiva, M. & Sabio, G. The role of stress kinases in metabolic disease. *Nat. Rev. Endocrinol.* **16**, 697–716 (2020).
10. Canovas, B. & Nebreda, A. R. Diversity and versatility of p38 kinase signalling in health and disease. *Nat. Rev. Mol. Cell Biol.* **22**, 346–366 (2021).
11. Romero-Becerra, R. et al. MKK6 deficiency promotes cardiac dysfunction through MKK3-p38γ/δ-mTOR hyperactivation. *eLife* **11**, e75250 (2022).
12. Romero-Becerra, R., Santamans, A., Folgueira, C. & Sabio, G. p38 MAPK pathway in the heart: new insights in health and disease. *Int. J. Mol. Sci.* **21**, 7412 (2020).
13. González-Terán, B. et al. P38γ and δ promote heart hypertrophy by targeting the mTOR-inhibitory protein DEPTOR for degradation. *Nat. Commun.* **7**, 10477 (2016).
14. Yan, J. et al. Stress signaling JNK2 crosstalk with CaMKII underlies enhanced atrial arrhythmogenesis. *Circ. Res.* **122**, 821–835 (2018).
15. Landstrom, A. P., Dobrev, D. & Wehrens, X. H. T. Calcium signaling and cardiac arrhythmias. *Circ. Res.* **120**, 1969–1993 (2017).
16. Patel, P. J., Segar, R., Patel, J. K., Padanilam, B. J. & Prystowsky, E. N. Arrhythmia induction using isoproterenol or epinephrine during electrophysiology study for supraventricular tachycardia. *J. Cardiovasc. Electrophysiol.* **29**, 1635–1640 (2018).
17. Bonne, G., Carrier, L., Richard, P., Hainque, B. & Schwartz, K. Familial hypertrophic cardiomyopathy. *Circ. Res.* **83**, 580–593 (1998).
18. Carrier, L. et al. Asymmetric septal hypertrophy in heterozygous cMyBP-C null mice. *Cardiovasc. Res.* **63**, 293–304 (2004).
19. Berul, C. I. et al. Ventricular arrhythmia vulnerability in cardiomyopathic mice with homozygous mutant myosin-binding protein C gene. *Circulation* **104**, 2734–2739 (2001).
20. Brayson, D. & Shanahan, C. M. Current insights into LMNA cardiomyopathies: existing models and missing LINC. *Nucleus* **8**, 17–33 (2017).
21. Santamans, A. M. et al. p38γ and p38δ regulate postnatal cardiac metabolism through glycogen synthase 1. *PLoS Biol.* **19**, e3001447 (2021).
22. Krämer, A., Green, J., Pollard, J. & Tugendreich, S. Causal analysis approaches in Ingenuity Pathway Analysis. *Bioinformatics* **30**, 523–530 (2014).
23. Bagwan, N. et al. Comprehensive quantification of the modified proteome reveals oxidative heart damage in mitochondrial heteroplasmy. *Cell Rep.* **23**, 3685–3697 (2018).
24. Priori, S. G. & Chen, S. R. W. Inherited dysfunction of sarcoplasmic reticulum Ca<sup>2+</sup> handling and arrhythmogenesis. *Circ. Res.* **108**, 871–883 (2011).
25. Dobrev, D. & Wehrens, X. H. T. Role of RyR2 phosphorylation in heart failure and arrhythmias. *Circ. Res.* **114**, 1311–1319 (2014).
26. Nerbonne, J. M. Mouse models of arrhythmogenic cardiovascular disease: challenges and opportunities. *Curr. Opin. Pharmacol.* **15**, 107–114 (2014).
27. Choy, L., Yeo, J. M., Tse, V., Chan, S. P. & Tse, G. Cardiac disease and arrhythmogenesis: mechanistic insights from mouse models. *Int. J. Cardiol. Heart Vasc.* **12**, 1–10 (2016).
28. Pandit, S. V. & Jalife, J. Rotors and the dynamics of cardiac fibrillation. *Circ. Res.* **112**, 849–862 (2013).
29. McCauley, M. D. & Wehrens, X. H. T. Targeting ryanodine receptors for anti-arrhythmic therapy. *Acta Pharmacol. Sin.* **32**, 749–757 (2011).
30. Campbell, H. M. et al. Loss of SPEG inhibitory phosphorylation of ryanodine receptor type-2 promotes atrial fibrillation. *Circulation* **142**, 1159–1172 (2020).
31. Zhao, Y.-T. et al. Arrhythmogenesis in a catecholaminergic polymorphic ventricular tachycardia mutation that depresses ryanodine receptor function. *Proc. Natl Acad. Sci. USA* **112**, E1669–E1677 (2015).
32. Li, Y. et al. Human RyR2 (ryanodine receptor 2) loss-of-function mutations: clinical phenotypes and in vitro characterization. *Circ. Arrhythm. Electrophysiol.* **14**, e010013 (2021).
33. Jiang, D. et al. RyR2 mutations linked to ventricular tachycardia and sudden death reduce the threshold for store-overload-induced Ca<sup>2+</sup> release (SOICR). *Proc. Natl Acad. Sci. USA* **101**, 13062–13067 (2004).
34. Bers, D. M. Calcium cycling and signaling in cardiac myocytes. *Annu. Rev. Physiol.* **70**, 23–49 (2008).
35. Scharf, M. et al. Mitogen-activated protein kinase-activated protein kinases 2 and 3 regulate SERCA2a expression and fiber type composition to modulate skeletal muscle and cardiomyocyte function. *Mol. Cell. Biol.* **33**, 2586–2602 (2013).
36. Choi, B. R., Burton, F. & Salama, G. Cytosolic Ca<sup>2+</sup> triggers early afterdepolarizations and torsade de pointes in rabbit hearts with type 2 long QT syndrome. *J. Physiol.* **543**, 615–631 (2002).
37. Chelu, M. G. et al. Calmodulin kinase II-mediated sarcoplasmic reticulum Ca<sup>2+</sup> leak promotes atrial fibrillation in mice. *J. Clin. Invest.* **119**, 1940–1951 (2009).
38. Zhao, Z. et al. Revisiting the ionic mechanisms of early afterdepolarizations in cardiomyocytes: predominant by Ca waves or Ca currents? *Am. J. Physiol. Heart Circ. Physiol.* **302**, 1636–1644 (2012).
39. Barry, D. M., Xu, H., Schuessler, R. B. & Nerbonne, J. M. Functional knockout of the transient outward current, long-QT syndrome, and cardiac remodeling in mice expressing a dominant-negative Kv4 α subunit. *Circ. Res.* **83**, 560–567 (1998).
40. El-Haou, S. et al. Kv4 potassium channels form a tripartite complex with the anchoring protein SAP97 and CaMKII in cardiac myocytes. *Circ. Res.* **104**, 758–769 (2009).
41. Sabio, G. et al. p38γ regulates the localisation of SAP97 in the cytoskeleton by modulating its interaction with GKAP. *EMBO J.* **24**, 1134–1145 (2005).
42. Nosedá, R. et al. Kif13b regulates PNS and CNS myelination through the Dlg1 scaffold. *PLoS Biol.* **14**, e1002440 (2016).
43. Morita, N., Mandel, W. J., Kobayashi, Y. & Karagueuzian, H. S. Cardiac fibrosis as a determinant of ventricular tachyarrhythmias. *J. Arrhythm.* **30**, 389–394 (2014).
44. Sohns, C. & Marrouche, N. F. Atrial fibrillation and cardiac fibrosis. *Eur. Heart J.* **41**, 1123–1131 (2020).
45. Yan, J. et al. c-Jun N-terminal kinase activation contributes to reduced connexin43 and development of atrial arrhythmias. *Cardiovasc Res* **97**, 589–597 (2013).
46. Zipes, D. P. et al. ACC/AHA/ESC 2006 guidelines for management of patients with ventricular arrhythmias and the prevention of sudden cardiac death. *J. Am. Coll. Cardiol.* **48**, e247–e346 (2006).
47. Merentie, M. et al. Efficacy and safety of myocardial gene transfer of adenovirus, adeno-associated virus and lentivirus vectors in the mouse heart. *Gene Ther.* **23**, 296–305 (2015).



48. Li, Z. et al. Age-induced augmentation of p38 MAPK phosphorylation in mouse lung. *Exp. Gerontol.* **46**, 694–702 (2011).
49. Preston, C. C. et al. Aging-induced alterations in gene transcripts and functional activity of mitochondrial oxidative phosphorylation complexes in the heart. *Mech. Ageing Dev.* **129**, 304–312 (2008).
50. Seppet, E. et al. Compartmentation of energy metabolism in atrial myocardium of patients undergoing cardiac surgery. *Mol. Cell. Biochem.* **270**, 49–61 (2005).
51. Morita, N. et al. Glycolytic inhibition causes spontaneous ventricular fibrillation in aged hearts. *Am. J. Physiol. Heart Circ. Physiol.* **301**, H180–H191 (2011).
52. Delise, P. & Sciarra, L. Sudden cardiac death in patients with ventricular preexcitation. *Card. Electrophysiol. Clin.* **12**, 519–525 (2020).
53. Brembilla-Perrot, B. et al. Inducible multiform ventricular tachycardia in Wolff–Parkinson–White syndrome. *Heart* **58**, 89–95 (1987).
54. Miyamoto, L. Molecular pathogenesis of familial Wolff–Parkinson–White Syndrome. *J. Med. Invest.* **65**, 1–8 (2018).
55. Li, J., Miller, E. J., Ninomiya-Tsuji, J., Russell, R. R. & Young, L. H. AMP-activated protein kinase activates p38 mitogen-activated protein kinase by increasing recruitment of p38 MAPK to TAB1 in the ischemic heart. *Circ. Res.* **97**, 872–879 (2005).
56. Matesanz, N. et al. MKK6 controls T3-mediated browning of white adipose tissue. *Nat. Commun.* **8**, 856 (2017).
57. Johnson, J. L. et al. An atlas of substrate specificities for the human serine/threonine kinome. *Nature* **613**, 759–766 (2023).
58. Wickenden, A. D. et al. The role of action potential prolongation and altered intracellular calcium handling in the pathogenesis of heart failure. *Cardiovasc. Res.* **37**, 312–323 (1998).
59. Gillet, L. et al. Cardiac-specific ablation of synapse-associated protein SAP97 in mice decreases potassium currents but not sodium current. *Heart Rhythm* **12**, 181–192 (2015).
60. Tinaquero, D. et al. The p.P888L SAP97 polymorphism increases the transient outward current ( $I_{to,t}$ ) and abbreviates the action potential duration and the QT interval. *Sci. Rep.* **10**, 10707 (2020).
61. Musa, H. et al. Abnormal myocardial expression of SAP97 is associated with arrhythmogenic risk. *Am. J. Physiol. Heart Circ. Physiol.* **318**, H1357–H1370 (2020).
62. Koura, T. et al. Anisotropic conduction properties in canine atria analyzed by high-resolution optical mapping. *Circulation* **105**, 2092–2098 (2002).
63. Yan, J. et al. The stress kinase JNK regulates gap junction Cx43 gene expression and promotes atrial fibrillation in the aged heart. *J. Mol. Cell. Cardiol.* **114**, 105–115 (2018).
64. Brancho, D. et al. Mechanism of p38 MAP kinase activation in vivo. *Genes Dev.* **17**, 1969–1978 (2003).
65. Hauswirth, W. W., Lewin, A. S., Zolotukhin, S. & Muzyczka, N. Production and purification of recombinant adeno-associated virus. *Methods Enzymol.* **316**, 743–761 (2000).
66. Schneider, C. A., Rasband, W. S. & Eliceiri, K. W. NIH Image to ImageJ: 25 years of image analysis. *Nat. Methods* **9**, 671–675 (2012).
67. Lian, X. et al. Directed cardiomyocyte differentiation from human pluripotent stem cells by modulating Wnt/ $\beta$ -catenin signaling under fully defined conditions. *Nat. Protoc.* **8**, 162–175 (2013).
68. Rivera-Torres, J. et al. Cardiac electrical defects in progeroid mice and Hutchinson–Gilford progeria syndrome patients with nuclear lamina alterations. *Proc. Natl Acad. Sci. USA* **113**, E7250–E7259 (2016).
69. Mitchell, G. F., Jeron, A. & Koren, G. Measurement of heart rate and Q-T interval in the conscious mouse. *Am. J. Physiol.* **274**, H747–H751 (1998).
70. Cerrone, M. et al. Arrhythmogenic mechanisms in a mouse model of catecholaminergic polymorphic ventricular tachycardia. *Circ. Res.* **101**, 1039–1048 (2007).
71. Noujaim, S. F. et al. Up-regulation of the inward rectifier  $K^+$  current ( $I_{K1}$ ) in the mouse heart accelerates and stabilizes rotors. *J. Physiol.* **578**, 315–326 (2007).
72. Li, N. & Wehrens, X. H. T. Programmed electrical stimulation in mice. *J. Vis. Exp.* 1730 (2010).
73. Samie, F. H. et al. Rectification of the background potassium current. *Circ. Res.* **89**, 1216–1223 (2001).
74. Zaitsev, A. V., Berenfeld, O., Mironov, S. F., Jalife, J. & Pertsov, A. M. Distribution of excitation frequencies on the epicardial and endocardial surfaces of fibrillating ventricular wall of the sheep heart. *Circ. Res.* **86**, 408–417 (2000).
75. Muñoz, V. et al. Adenoviral expression of  $I_{Ks}$  contributes to wavebreak and fibrillatory conduction in neonatal rat ventricular cardiomyocyte monolayers. *Circ. Res.* **101**, 475–483 (2007).
76. Cardona, M. et al. Executioner caspase-3 and 7 deficiency reduces myocyte number in the developing mouse heart. *PLoS ONE* **10**, e0131411 (2015).
77. Martínez-Bartolomé, S. et al. Properties of average score distributions of SEQUEST: the probability ratio method. *Mol. Cell. Proteomics* **7**, 1135–1145 (2008).
78. Navarro, P. & Vázquez, J. A refined method to calculate false discovery rates for peptide identification using decoy databases. *J. Proteome Res.* **8**, 1792–1796 (2009).
79. Bonzon-Kulichenko, E., Garcia-Marques, F., Trevisan-Herraz, M. & Vázquez, J. Revisiting peptide identification by high-accuracy mass spectrometry: problems associated with the use of narrow mass precursor windows. *J. Proteome Res.* **14**, 700–710 (2015).
80. Rodríguez, J. M. et al. iSanXoT: a standalone application for the integrative analysis of mass spectrometry-based quantitative proteomics data. Preprint at *bioRxiv* <https://doi.org/10.1101/2023.08.25.554773> (2023).
81. Trevisan-Herraz, M. et al. SanXoT: a modular and versatile package for the quantitative analysis of high-throughput proteomics experiments. *Bioinformatics* **35**, 1594–1596 (2019).
82. Navarro, P. et al. General statistical framework for quantitative proteomics by stable isotope labeling. *J. Proteome Res.* **13**, 1234–1247 (2014).
83. García-Marqués, F. et al. A novel systems-biology algorithm for the analysis of coordinated protein responses using quantitative proteomics. *Mol. Cell. Proteomics* **15**, 1740–1760 (2016).
84. Ritchie, M. E. et al. limma powers differential expression analyses for RNA-seq and microarray studies. *Nucleic Acids Res.* **43**, e47 (2015).
85. Hornbeck, P. V. et al. PhosphoSitePlus, 2014: mutations, PTMs and recalibrations. *Nucleic Acids Res.* **43**, D512–D520 (2015).
86. Perez-Riverol, Y. et al. The PRIDE database resources in 2022: a hub for mass spectrometry-based proteomics evidences. *Nucleic Acids Res.* **50**, D543–D552 (2022).
87. Doncheva, N. T., Morris, J. H., Gorodkin, J. & Jensen, L. J. Cytoscape StringApp: network analysis and visualization of proteomics data. *J. Proteome Res.* **18**, 623–632 (2019).
88. Legeay, M., Doncheva, N. T., Morris, J. H. & Jensen, L. J. Visualize omics data on networks with Omics Visualizer, a Cytoscape app. *F1000Res.* **9**, 157 (2020).
89. Shannon, P. et al. Cytoscape: a software environment for integrated models of biomolecular interaction networks. *Genome Res.* **13**, 2498–2504 (2003).

## Acknowledgements

We gratefully acknowledge L. Sen-Martín, J. Alegre-Cebollada (CNIC, Madrid) and L. Carrier (University Medical Center Hamburg-Eppendorf and DZHK, Hamburg) for the cMyBP3-C KO cardiac tissue;



D. Roiz-Valle and C. López-Otín (IUOPA; Universidad de Oviedo, Oviedo) for the *Lmna*<sup>G609G/G609G</sup> cardiac tissue; and R. J. Davis for the MKK6 KO mice. We thank G. Giovinazzo and the CNIC Pluripotent Cell Technology Unit (CNIC, Madrid) for the hiPSCs. We thank S. Bartlett and F. Chanut (CNIC, Madrid) for English editing, and R. R. Mondragon (University of Michigan, Ann Arbor) for technical support. We are grateful to R. J. Davis (University of Massachusetts Chan Medical School, Worcester), A. Padmanabhan (University of California, San Francisco) and M. Costa and C. López-Otín (IUOPA; Universidad de Oviedo, Oviedo) for critical reading of the manuscript. We thank the staff at the CNIC Genomics and Bioinformatics Units for technical support and help with data analysis and A. C. Silva for help with figure editing and design. This work was funded by a CNIC Intramural Project Severo Ochoa (Expediente 12-2016 IGP) to G.S. and J.J. G.S. is supported by the following projects: PMP21/00057 IMPACT-2021, funded by the Instituto de Salud Carlos III (ISCIII), and PDC2021-121147-I00 and PID2019-104399RB-I00, funded by MCIN/AEI/10.13039/501100011033—all funded by the European Union (FEDER/FSE); ‘Una manera de hacer Europa’/‘El FSE invierte en tu futuro’/Next Generation EU and co-funded by the European Union/Plan de Recuperación, Transformación y Resiliencia (PRTR). R.R.B. is a fellow of the FPU Program (FPU17/03847). B.G.T. was a fellow of the FPI Severo Ochoa CNIC Program (SVP-2013-067639) and an American Heart Association Postdoctoral Fellow (18POST34080175). The following grants provided additional funding: Instituto de Salud Carlos III, PDC2021-121147-I00 Convocatoria: Proyectos Prueba de Concepto 2021 Ministerio de Ciencia e Innovación and PID2022-138525OB-I00 Ministerio de Ciencia e Innovación; US National Heart, Lung, and Blood Institute (R01 grant HL122352); Fondos FEDER, Madrid, Spain, and Fundación Bancaria ‘La Caixa (project HR19/52160013) to J.J.; American Heart Association Postdoctoral Fellowship 14POST17820005 to D.P.B.; and MICINN PGC2018-097019-B-I00, ISCIII-SGEFI/ERDF (PRB3-IPT17/0019, ProteoRed), the Fundació Marató TV3 (grant 122/C/2015) and ‘la Caixa’ Banking Foundation (project code HR17-00247) to J.V. The CNIC is supported by the Instituto de Salud Carlos III (ISCIII), the Ministerio de Ciencia e Innovación (MCIN) and the Pro CNIC Foundation and is a Severo Ochoa Center of Excellence (grant CEX2020-001041-S, funded by MICIN/AEI/10.13039/501100011033).

### Author contributions

G.S. conceived this project. G.S. and J.J. supervised this project. R.R.-B. performed the primary experiments, acquired and analyzed the data and prepared figures. G.S., J.J. and R.R.-B. designed the study,

developed the hypothesis and wrote the paper, with input from all authors. J.A.L. and J.V. performed the phosphoproteomics analysis. R.R.-B. performed the bioinformatic analysis. D.P.-B., A.A., F.M.C.U., R.R.-M, G.G.-S. and E.N.J.-V. performed cardiomyocyte isolation, patch-clamp experiments, optical mapping and in vivo intracardiac catheter burst pacing. A.M., B.G.-T., M.L., M.E.R. and L.L.-V. help to perform some of the experiments and acquired data. D.F.-R. analyzed the ECG recordings and critically revised the paper. J.J. and G.S. led and funded the project.

### Competing interests

The authors declare no competing interests.

### Additional information

**Extended data** is available for this paper at <https://doi.org/10.1038/s44161-023-00368-x>.

**Supplementary information** The online version contains supplementary material available at <https://doi.org/10.1038/s44161-023-00368-x>.

**Correspondence and requests for materials** should be addressed to José Jalife or Guadalupe Sabio.

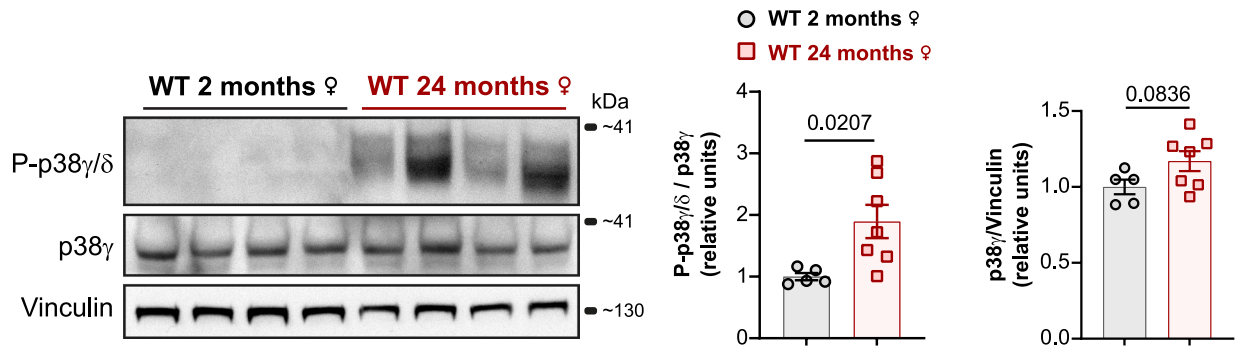
**Peer review information** *Nature Cardiovascular Research* thanks Xander Wehrens and the other, anonymous, reviewers for their contribution to the peer review of this work. Primary Handling Editor: Elvira Forte, in collaboration with the *Nature Cardiovascular Research* team.

**Reprints and permissions information** is available at [www.nature.com/reprints](http://www.nature.com/reprints).

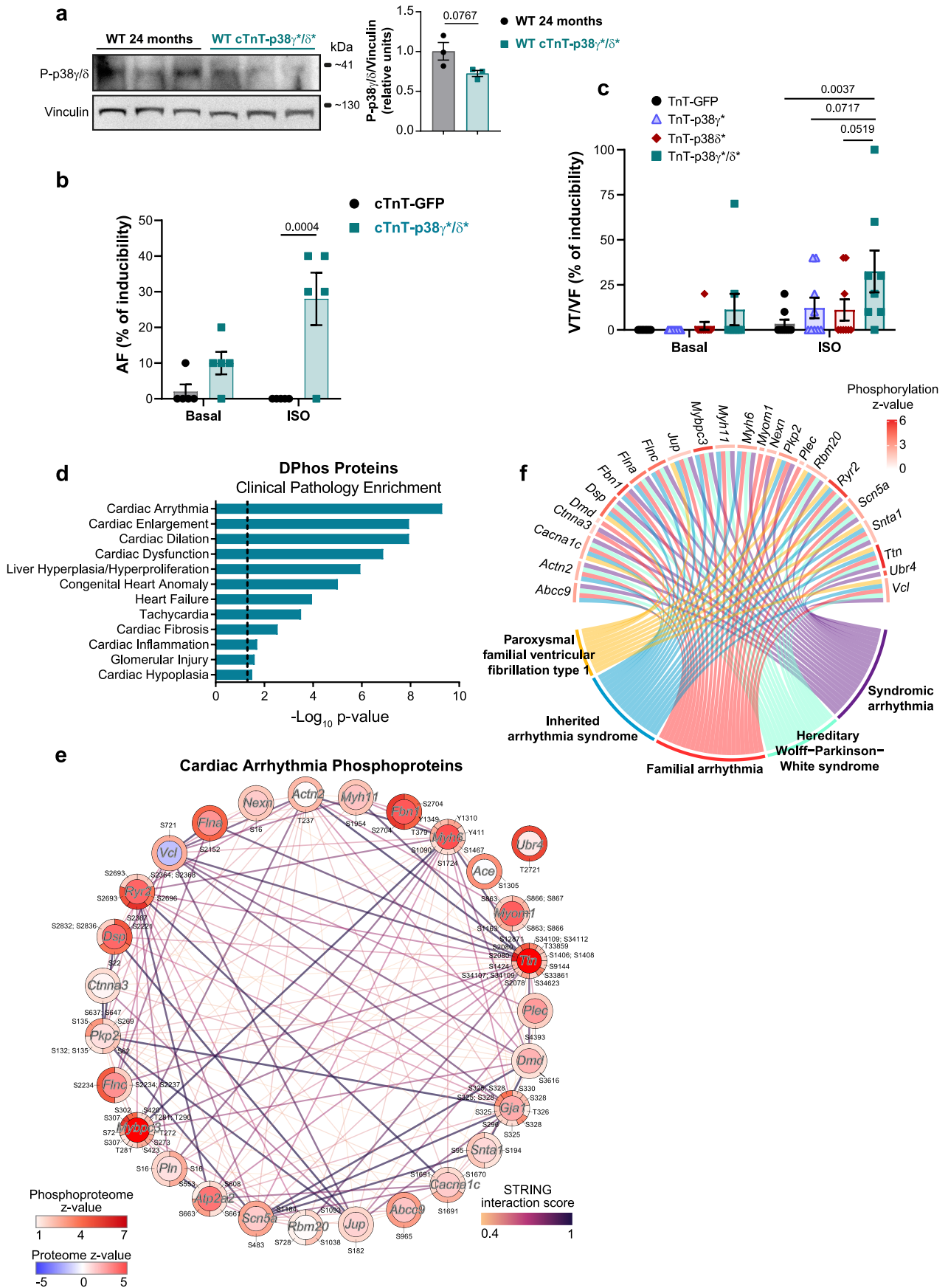
**Publisher’s note** Springer Nature remains neutral with regard to jurisdictional claims in published maps and institutional affiliations.

Springer Nature or its licensor (e.g. a society or other partner) holds exclusive rights to this article under a publishing agreement with the author(s) or other rightsholder(s); author self-archiving of the accepted manuscript version of this article is solely governed by the terms of such publishing agreement and applicable law.

© The Author(s), under exclusive licence to Springer Nature Limited 2023



**Extended Data Fig. 1 | p38γ/δ have increased phosphorylation levels in hearts from old female WT mice.** Immunoblot analysis of the phosphorylation and protein levels of p38γ/δ in heart lysates from 2-month-old ( $n=5$ ) and 24-month-old ( $n=7$ ) female mice. Two-sided unpaired Student's t-test. Data are expressed as mean  $\pm$  SEM.

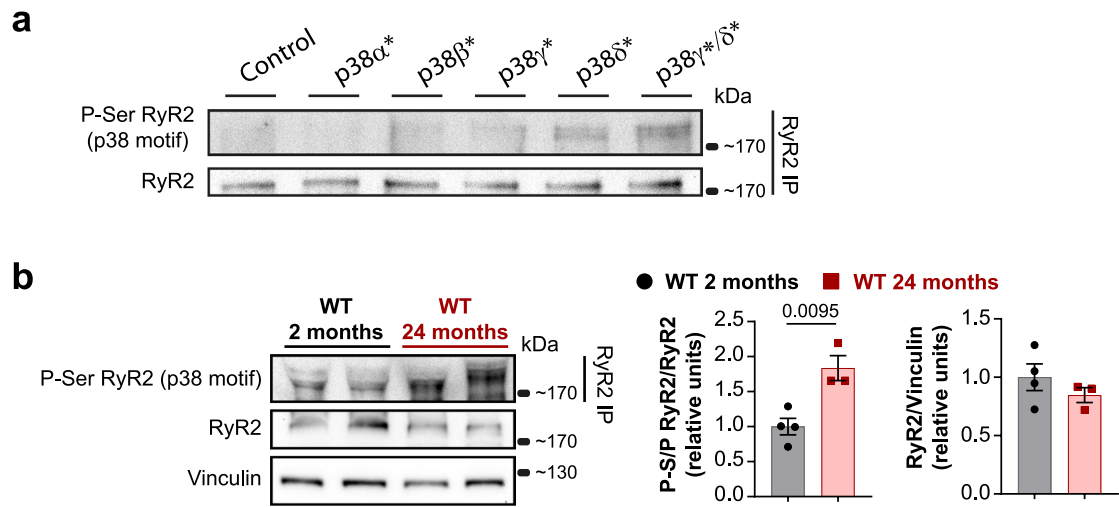


Extended Data Fig. 2 | See next page for caption.

**Extended Data Fig. 2 | Cardiac arrhythmia phosphoproteome network in cTnT-p38 $\gamma$ / $\delta$ \* hearts.** **a**, Phosphorylation levels of p38 $\gamma$ / $\delta$  assessed by immunoblot in heart lysates from 24-month-old WT ( $n = 3$ ) and cTnT-p38 $\gamma$ / $\delta$ \* ( $n = 3$ ) mice. Two-sided unpaired Student's t-test. **b**, Percentage of atrial fibrillation (AF) inducibility by S1-S2 protocol 1 in the absence (basal) and presence (ISO) of isoproterenol (i.p. 5 mg/kg) in 2-month-old cTnT-GFP ( $n = 5$ ) and cTnT-p38 $\gamma$ / $\delta$ \* ( $n = 5$ ) male mice. Each dot shows the percentage of AF induced in each mouse by the S1-S2 protocol 1. 2-way ANOVA followed by Sidak's post-test. **c**, Percentage of VT/VF inducibility by S1-S2 protocol 1 in cTnT-GFP ( $n = 9$ ), cTnT-p38 $\gamma$ \* ( $n = 9$ ), cTnT-p38 $\delta$ \* ( $n = 9$ ) and cTnT-p38 $\gamma$ / $\delta$ \* ( $n = 8$ ) mice in the absence (basal) and presence (ISO) of isoproterenol (i.p. 5mg/kg). Each dot shows the percentage of VT/VF induced in each mouse by the S1-S2 protocol 1. 2-way ANOVA followed by Tukey's post-test. Data are expressed as mean  $\pm$  SEM. **d**, Clinical Pathology Enrichment (Tox Functions) of the differentially hyperphosphorylated proteins ( $z$ -value difference  $> 0$ ; limma two-sided t-test  $p$ -value  $< 0.05$ ) from cTnT-p38 $\gamma$ / $\delta$ \* hearts non-corrected phosphoproteome

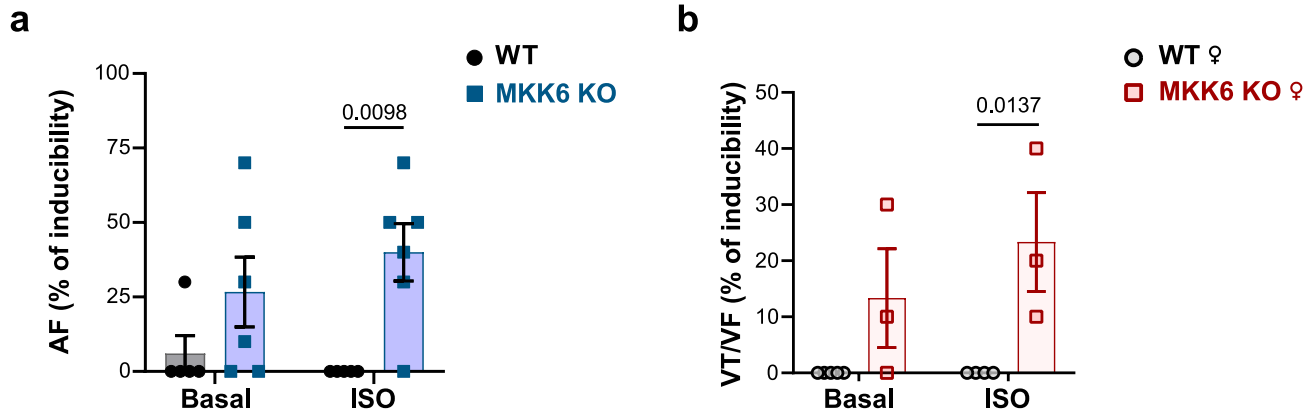
compared to controls, as determined by Ingenuity Pathway Analysis. The vertical dashed line indicates the threshold of  $-\text{Log}_{10}$  (Two-sided Fisher's exact test  $p$ -value) = 1.3. **e**, Interaction network of DPhos proteins involved in the category 'Cardiac Arrhythmia' shown in (d), based on STRING database, and visualized in Cytoscape. The node colors indicate the differential abundance (inner circle) and phosphorylation state (outer circle) of the proteins in cTnT-p38 $\gamma$ / $\delta$ \* vs cTnT-GFP hearts. Small numbers pointing to segments of the outer circles indicate the position of the phosphosite in the sequence of the protein. The edge colors indicate the STRING interaction score between proteins. Only significant ( $z$ -value difference  $> 0$ ; limma two-sided t-test  $p$ -value  $< 0.05$ ) phosphopeptides are indicated. Proteins are defined by their gene name for simplicity. **f**, Chord diagram of the phosphoproteins found in the category 'Cardiac Arrhythmia' shown in (d), and the 5 most significant pathologies in this category to which the phosphoproteins are assigned. Proteins are identified by their gene name for simplicity. Data are expressed as mean  $\pm$  SEM.





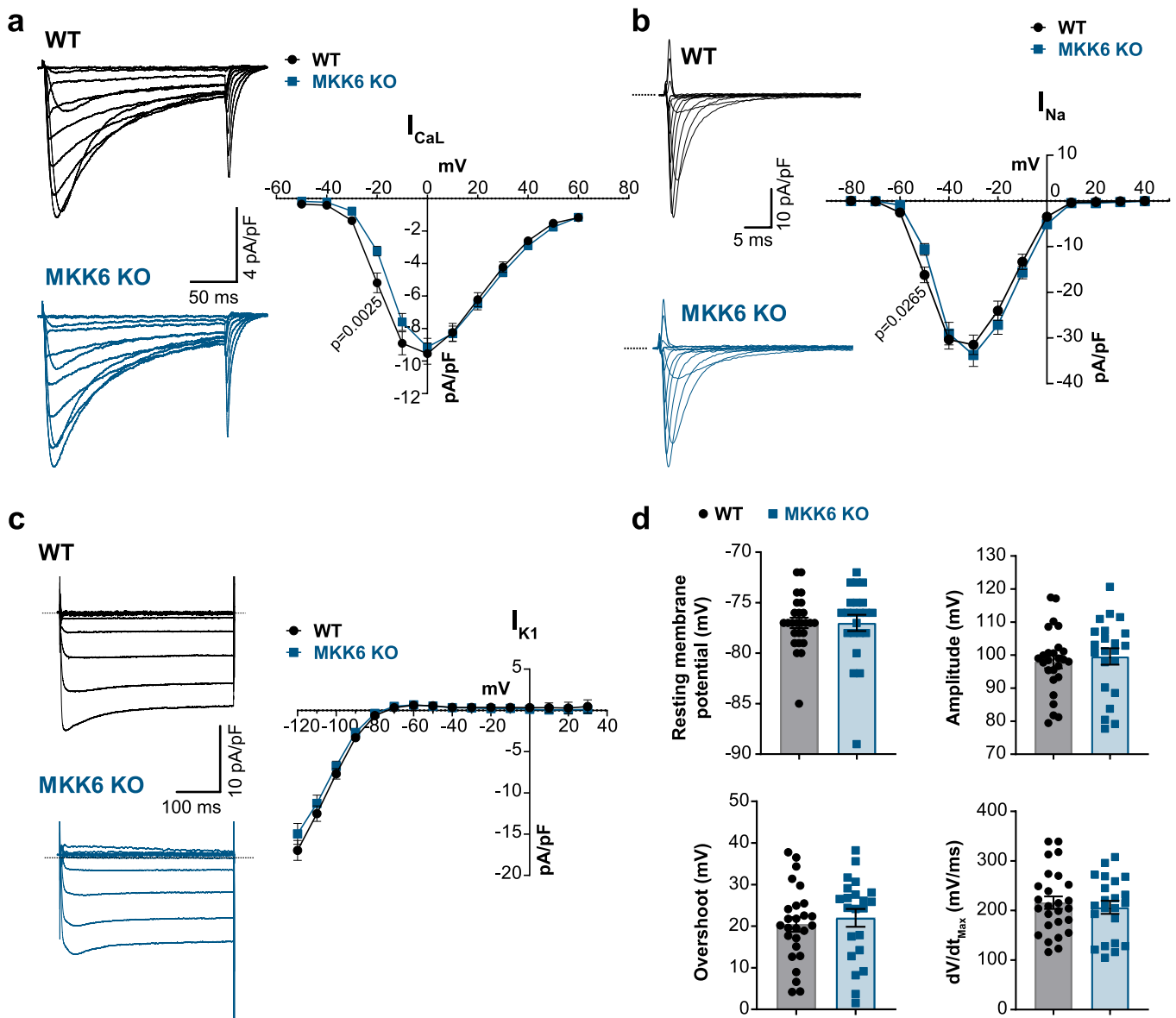
**Extended Data Fig. 3 | p38 $\gamma$ / $\delta$  activity is related to phosphorylation of RyR2 at p-Ser p38 motif.** **a**, Representative blot of two independent in vitro phosphorylation kinase assays of RyR2 isolated from mice hearts on P-Ser p38 motif by active-recombinant p38 $\alpha$ , p38 $\beta$ , p38 $\gamma$ , p38 $\delta$ , and p38 $\gamma$  and p38 $\delta$

together. **b**, Immunoblot analysis of RyR2 phosphorylation at P-Ser p38 motif in heart lysates from 2-month-old ( $n=4$ ) and 24-month-old ( $n=3$ ) WT mice. Two-sided unpaired Student's t-test. Data are expressed as mean  $\pm$  SEM.



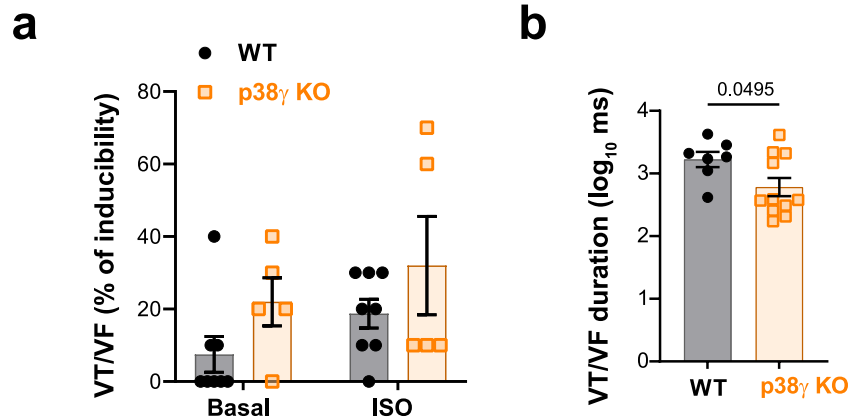
**Extended Data Fig. 4 | p38 $\gamma$ / $\delta$  activation due to MKK6 deficiency promotes atrial fibrillation and also ventricular arrhythmias independently of the sex. **a**, Percentage of atrial fibrillation (AF) inducibility by S1-S2 protocol 1 in the absence (basal) and presence (ISO) of isoproterenol (i.p. 5 mg/kg) in 5-month-old WT ( $n=5$ ) and MKK6 KO ( $n=6$ ) male mice. **b**, Percentage of VT/VF inducibility**

by S1-S2 protocol 1 in WT ( $n=4$ ) and MKK6 KO ( $n=3$ ) female mice in the absence (basal) and presence (ISO) of isoproterenol (i.p. 5 mg/kg). Each dot shows the percentage of AF (a) or VT/VF (b) induced in each mouse by the S1-S2 protocol 1. 2-way ANOVA followed by Sidak's post-test. Data are expressed as mean  $\pm$  SEM.



**Extended Data Fig. 5 |  $I_{CaL}$ ,  $I_{Na}$  and  $I_{K1}$  in 2-month-old WT and MKK6 KO cardiomyocytes.** **a**, Representative  $I_{CaL}$  traces (left) and  $I_{CaL}$  I/V relationship (right) from 2-month-old WT ( $n=21$ ) and MKK6 KO ( $n=22$ ) cardiomyocytes. Mean peak current densities at -0 mV were  $-9 \pm 0.5$  (WT) versus  $-8 \pm 0.6$  (MKK6 KO) pA/pF. 2-way ANOVA followed by Sidak's post-test. Data were collected from 3 independent cardiomyocyte isolation for each condition. **b**, Representative sodium current traces (left) and  $I_{Na}$  I/V relationship (right) in WT ( $n=22$ ) and MKK6 KO ( $n=28$ ) cardiomyocytes.  $I_{Na}$  densities at -30 mV were similar in both groups ( $-31 \pm 2$  pA/pF in WT vs  $-33 \pm 2$  pA/pF in MKK6 KO cardiomyocytes). 2-way ANOVA followed by Sidak's post-test. Data were collected from 5 independent

cardiomyocyte isolation for each condition. **c**, Representative  $I_{K1}$  current traces (left) and  $I_{K1}$  I/V relationship (right) from WT ( $n=10$ ) and MKK6 KO ( $n=9$ ) cardiomyocytes. Mean peak current densities at -120 mV were  $-14 \pm 1.1$  (WT) versus  $-16 \pm 1.1$  (MKK6 KO) pA/pF. 2-way ANOVA followed by Sidak's post-test. Data were collected from 3 independent cardiomyocyte isolation for each condition. **d**, Resting membrane potential, action potential amplitude, overshoot, and maximum rate of action potential depolarization ( $dV/dt_{max}$ ) in WT ( $n=26$ ) and MKK6 KO ( $n=22$ ) cardiomyocytes. Two-sided unpaired Student's t-test or Mann-Whitney U test. Data were collected from 4 independent cardiomyocyte isolation for each condition. Data are expressed as mean  $\pm$  SEM.



**Extended Data Fig. 6 | Stress-induced arrhythmia burden in 9–10-month-old WT and p38 $\gamma$  KO mice. a**, Percentage of VT/VF inducibility by S1-S2 protocol 1 in 9–10-month-old WT ( $n = 8$ ) and p38 $\gamma$  KO ( $n = 5$ ) female mice in the absence (basal) and presence (ISO) of isoproterenol (i.p. 5 mg/kg). Each dot shows the percentage of VT/VF induced in each mouse by the S1-S2 protocol. 2-way ANOVA followed by

Tukey's post test. **b**, VT/VF duration in WT ( $n = 7$  VT/VF) and p38 $\gamma$  KO ( $n = 11$  VT/VF) female mice in basal condition. Each dot represents the duration of each induced arrhythmia. Two-sided unpaired Student's t-test. Data are expressed as mean  $\pm$  SEM.



## Reporting Summary

Nature Portfolio wishes to improve the reproducibility of the work that we publish. This form provides structure for consistency and transparency in reporting. For further information on Nature Portfolio policies, see our [Editorial Policies](#) and the [Editorial Policy Checklist](#).

### Statistics

For all statistical analyses, confirm that the following items are present in the figure legend, table legend, main text, or Methods section.

- | n/a                                 | Confirmed  |
|-------------------------------------|--|
| <input type="checkbox"/>            | <input checked="" type="checkbox"/> The exact sample size ( $n$ ) for each experimental group/condition, given as a discrete number and unit of measurement  |
| <input type="checkbox"/>            | <input checked="" type="checkbox"/> A statement on whether measurements were taken from distinct samples or whether the same sample was measured repeatedly  |
| <input type="checkbox"/>            | <input checked="" type="checkbox"/> The statistical test(s) used AND whether they are one- or two-sided<br><i>Only common tests should be described solely by name; describe more complex techniques in the Methods section.</i>   |
| <input type="checkbox"/>            | <input checked="" type="checkbox"/> A description of all covariates tested   |
| <input type="checkbox"/>            | <input checked="" type="checkbox"/> A description of any assumptions or corrections, such as tests of normality and adjustment for multiple comparisons  |
| <input type="checkbox"/>            | <input checked="" type="checkbox"/> A full description of the statistical parameters including central tendency (e.g. means) or other basic estimates (e.g. regression coefficient) AND variation (e.g. standard deviation) or associated estimates of uncertainty (e.g. confidence intervals) |
| <input type="checkbox"/>            | <input checked="" type="checkbox"/> For null hypothesis testing, the test statistic (e.g. $F$ , $t$ , $r$ ) with confidence intervals, effect sizes, degrees of freedom and $P$ value noted<br><i>Give <math>P</math> values as exact values whenever suitable.</i>                            |
| <input checked="" type="checkbox"/> | <input type="checkbox"/> For Bayesian analysis, information on the choice of priors and Markov chain Monte Carlo settings  |
| <input checked="" type="checkbox"/> | <input type="checkbox"/> For hierarchical and complex designs, identification of the appropriate level for tests and full reporting of outcomes  |
| <input checked="" type="checkbox"/> | <input type="checkbox"/> Estimates of effect sizes (e.g. Cohen's $d$ , Pearson's $r$ ), indicating how they were calculated  |

*Our web collection on [statistics for biologists](#) contains articles on many of the points above.*

### Software and code

Policy information about [availability of computer code](#)

**Data collection**

Electrocardiographic data were collected using the MP36R data acquisition unit and AcqKnowledge 4.1.0 software (BIOPAC Systems). Data were stored for offline analysis using custom scripts in MatLab for pre-processing, visualization, and quantification of electrophysiological intervals and heart rate variability.

Proteomics data were collected using a Q Exactive HF Orbitrap mass spectrometer (Thermo Fisher).

Electrophysiology experiments of mice free wall left ventricular cardiomyocytes were carried out using a Multiclamp 700B amplifier (Molecular Devices, Sunnyvale, CA, USA). Data were acquired and analyzed using the pCLAMP 10 (Molecular Devices, Sunnyvale, CA, USA). Action potential properties were analyzed using custom-made software developed by Krzysztof Grzeda for the Center of Arrhythmia Research, University of Michigan. Maximum upstroke velocity  $dV/dt_{max}$  was estimated using OriginPro 9 (OriginLab Corporation).

**Data analysis**

Western blot images were analyzed and quantified using ImageJ V1.53t.

Data from mass spectrometry were analyzed using the Proteome Discoverer version 2.1 and SEQUEST HT (Thermo Fisher Scientific). Statistical analysis was performed using GraphPad Prism 8.4.0 software.

For proteomics peptide identification, all spectra were analyzed with Proteome Discoverer (version 2.1.0.81, Thermo Fisher Scientific) using SEQUEST-HT (Thermo Fisher Scientific).

Phosphoproteomics analysis was performed using Ingenuity Pathway Analysis (July 2022 release, QIAGEN) and stringApp (1) and Omics Visualizer (2) within the Cytoscape software (3).

The sequence localization of phosphosites from proteins in the cardiac arrhythmia category was assigned consulting PhosphoSitePlus® (v6.6.0.4.) (4)

(1): Doncheva, N. T., Morris, J. H., Gorodkin, J. & Jensen, L. J. Cytoscape StringApp: Network Analysis and Visualization of Proteomics Data. J

Proteome Res 18, 623–632 (2019).

(2): Legeay, M., Doncheva, N. T., Morris, J. H., Jensen, L. J. & Palmblad, M. Visualize omics data on networks with Omics Visualizer, a Cytoscape App. *F1000Research* 2020 9:157 9, 157 (2020).

(3): Shannon, P. et al. Cytoscape: A Software Environment for Integrated Models of Biomolecular Interaction Networks. *Genome Res* 13, 2498–2504 (2003).

(4): Hornbeck, P. v. et al. PhosphoSitePlus, 2014: mutations, PTMs and recalibrations. *Nucleic Acids Res* 43, D512–D520 (2015).

For manuscripts utilizing custom algorithms or software that are central to the research but not yet described in published literature, software must be made available to editors and reviewers. We strongly encourage code deposition in a community repository (e.g. GitHub). See the Nature Portfolio [guidelines for submitting code & software](#) for further information.

## Data

Policy information about [availability of data](#)

All manuscripts must include a [data availability statement](#). This statement should provide the following information, where applicable:

- Accession codes, unique identifiers, or web links for publicly available datasets
- A description of any restrictions on data availability
- For clinical datasets or third party data, please ensure that the statement adheres to our [policy](#)

The mass spectrometry proteomics data have been deposited to the ProteomeXchange Consortium via the PRIDE partner repository with the dataset identifier PXD045996.

## Human research participants

Policy information about [studies involving human research participants and Sex and Gender in Research](#).

Reporting on sex and gender

Population characteristics

Recruitment

Ethics oversight

Note that full information on the approval of the study protocol must also be provided in the manuscript.

## Field-specific reporting

Please select the one below that is the best fit for your research. If you are not sure, read the appropriate sections before making your selection.

Life sciences  Behavioural & social sciences  Ecological, evolutionary & environmental sciences

For a reference copy of the document with all sections, see [nature.com/documents/nr-reporting-summary-flat.pdf](https://www.nature.com/documents/nr-reporting-summary-flat.pdf)

## Life sciences study design

All studies must disclose on these points even when the disclosure is negative.

Sample size

Data exclusions

Replication

Randomization

Blinding

# Reporting for specific materials, systems and methods

We require information from authors about some types of materials, experimental systems and methods used in many studies. Here, indicate whether each material, system or method listed is relevant to your study. If you are not sure if a list item applies to your research, read the appropriate section before selecting a response.

## Materials & experimental systems

- n/a  Involved in the study
- Antibodies
- Eukaryotic cell lines
- Palaeontology and archaeology
- Animals and other organisms
- Clinical data
- Dual use research of concern

## Methods

- n/a  Involved in the study
- ChIP-seq
- Flow cytometry
- MRI-based neuroimaging

## Antibodies

Antibodies used	SAP97 (DU391) (MRC PPU) at 1 µg/mL; vinculin (Sigma) at 1:5000 dilution; MKK6 (#9264S), phospho-p38 MAPK (Thr180/Tyr182) (#9211S), phospho-MAPK/CDK Substrates (34B2) (#2325S), phospho-Threonine-Proline (P-Thr-Pro-101) (#9391S), p38 $\beta$ MAPK (#2307S), Phospho-Phospholamban (Ser16/Thr17) (#8496) (Cell Signaling Technology); RyR (F-1) (sc-376507), p38 $\alpha$ (C-20) (sc-535-G), SERCA2 (IID8) (sc-53010), GAPDH (FL-335) (sc-25778) (Santa Cruz Biotechnology); RyR2 (C3-33) (MA3-916), phospho-p38 MAPK gamma/delta (Tyr185, Tyr182) (PA5-105907) (ThermoFisher Scientific); Kv4.3 (75-017) (Neuromab); Caveolin 3 (610420) (BD Biosciences) all at a 1:1000 dilution. Phospho-PLN (Thr 17) (A010-13) and PLN (A010-14) from Badrilla at 1:5000 dilution.
Validation	All antibodies used were validated in the manufacturer's website for our species and application.

## Eukaryotic cell lines

Policy information about [cell lines and Sex and Gender in Research](#)

Cell line source(s)	hiPSC derived cardiomyocytes were obtained from WT hiPSC line HDF-iPS-SV10 (Spanish National Stem Cell Bank, ISCIII). All the information regarding this cell line can be obtained at <a href="https://www.isciii.es/QueHacemos/Servicios/BIOBANCOS/BNLC/Lists/Lneas%20iPS/Attachments/170/Caracteristicas%20-%20Documento_Deposito_Lineas_HDF-iPS-SV10-v2-f.pdf">https://www.isciii.es/QueHacemos/Servicios/BIOBANCOS/BNLC/Lists/Lneas%20iPS/Attachments/170/Caracteristicas%20-%20Documento_Deposito_Lineas_HDF-iPS-SV10-v2-f.pdf</a>
Authentication	NA (this study only involved the use of WT hiPSC line HDF-iPS-SV10)
Mycoplasma contamination	Cells were tested to confirm absence of Mycoplasma contamination (MycAlert PLUS Mycoplasma Detection Kit, Lonza).
Commonly misidentified lines (See <a href="#">ICLAC</a> register)	No commonly misidentified cell line was used in the study.

## Animals and other research organisms

Policy information about [studies involving animals; ARRIVE guidelines](#) recommended for reporting animal research, and [Sex and Gender in Research](#)

Laboratory animals	Wild-type animals were from the strain C57BL/6J (code:000664). MKK6 KO mice (B6.129-Map2k6tm1Flv) and MKK6/p38 $\gamma$ DKO (B6.129-Map2k6tm1Flv; B6.129-Mapk12tm1) were backcrossed for 10 generations or more to the C57BL/6J background. Male or female animals were used depending on the experiment, and the sex used for each experiment is specified in the figure legends. The animals were between 2 months (9-11 weeks) old and 24 months (105 weeks) old. The age of the animals used for each experiment is specified in the figure legends.
Wild animals	This study did not involve wild animals.
Reporting on sex	We checked that the phosphorylation of p38 $\gamma$ occurred in old mice in both sexes, as well as the susceptibility to arrhythmia in male and female MKK6 KO mice. After that, as there were not differences between sexes, we used males.
Field-collected samples	This study did not involve field-collected samples.
Ethics oversight	All animal procedures were approved by the CNIC Ethics Committee and the Madrid regional authorities (ref. PROEX 215/18) and conformed to EU Directive 86/609/EEC and Recommendation 2007/526/EC regarding the protection of animals used for experimental and other scientific purposes, enacted under Spanish law Real Decreto 53/2013.

Note that full information on the approval of the study protocol must also be provided in the manuscript.